

A generalized echo squeezing protocol with near-Heisenberg limit sensitivity and strong robustness against excess noise and variation in squeezing parameter

Jinyang Li¹, Gregório R. M. da Silva¹, Schuyler Kain¹, Selim M. Shahriar^{2,3}

¹ Department of Physics and Astronomy, Northwestern University, Evanston, IL 60208, USA

² Department of ECE, Northwestern University, Evanston, IL 60208, USA

³ Digital Optics Technologies, Rolling Meadows, IL 60008, USA

Abstract

We present a generalized echo squeezing protocol (GESP) as a generalization of the Schrödinger cat state protocol (SCSP) with the value of the squeezing parameter being an arbitrary number rather than $\pi/2$. We show analytically that over a very broad range of the squeezing parameter the sensitivity of the GESP reaches the Heisenberg limit within a factor of $\sqrt{2}$. For a large number of atoms, N , this plateau interval is almost the whole range from zero to $\pi/2$, and the sensitivity is independent of the parity of N . Therefore, it is possible to operate a sensor over a wide interval of the squeezing parameter without changing the sensitivity. This is to be contrasted with the conventional echo squeezing protocol (CESP) which only works for a very small interval of the squeezing parameter. We also show that, in contrast to the CESP, the sensitivity of the GESP is close to the quantum Cramér-Rao bound over the whole range of the squeezing parameter, indicating that the phase shift information contained in the quantum state is near-optimally extracted. We find that the enhancement in sensitivity in the case of the GESP is due to a combination of two parameters: the phase magnification factor (PMF) and the noise amplification factor (NAF). As the value of the squeezing parameter increases, both PMF and NAF increase, while keeping the ratio of PMF/NAF essentially constant, yielding a net enhancement of sensitivity at the Heisenberg limit within a factor of $\sqrt{2}$ over the whole plateau interval. An important consequence of this behavior is that the robustness of the GESP against excess noise easily exceeds that of the CESP for a broad range of values of the squeezing parameter. As such, in the context of an experimental study, it should be possible to achieve a net enhancement in sensitivity higher than that for the CESP, under typical conditions where the excess noise exceeds the quantum projection noise for the protocol without spin squeezing. Finally, we consider the fragility of the GESP against collisions with background particles, and show how a balance between the fragility and the robustness against excess noise would in practice determine the optimal choice of parameters for the GESP.

1. Introduction

The conventional echo squeezing protocol (CESP) [1,2] is a method of enhancing the sensitivity of an atomic sensor using one-axis-twist spin squeezing (OATS) [3,4,5,6,7,8,9]. The Hamiltonian for OATS can be expressed as χS_z^2 , where χ represents the strength of the non-linear interaction, and S_z is the sum of the z -components of the pseudo-spin vector for each atom, represented as a two level system. The effect of the OATS process on the collective response of the atoms is determined by the squeezing parameter, define as $\mu \equiv \chi t$, where t is the squeezing interaction time. The CESP can be applied to an atomic clock as well as a light-pulse atomic interferometer. For concreteness, we restrict the discussion here to the case of a Ramsey atomic clock. In summary, the CESP enhanced Ramsey clock works as follows [10]. We presume that the atoms are first prepared in the state where all the pseudo-spinors are in the z -direction. We further assume that the first $\pi/2$ pulse causes a rotation around the y -axis, thus making all pseudo-spins point in the x -direction. This is followed by the OATS process, applied for an optimal value of $\mu \approx N^{-1/2}$, where N is the number of atoms being interrogated. Next, an auxiliary rotation, by an angle of $\pi/2$, is carried out around the x -axis, before the evolution during the dark period. At the end of the dark period, the auxiliary rotation is reversed, and the OATS process is applied again, with the sign of the squeezing Hamiltonian reversed (hence the use of the word “echo”). This is followed by another $\pi/2$ pulse, but around the x -axis, rather than the y -axis. The signal measured is the expectation value of S_z . It has been shown [1] that, under ideal conditions, the sensitivity is enhanced by a factor of $\sim \sqrt{N/e}$. It has also been shown [1,2] that this enhancement is due only to a phase magnification, without any suppression of the quantum projection noise. A more detailed analysis [1] has shown than when sources of noise resulting from the cavity-based

approach for realizing the OATS process are taken into account, the actual factor of enhancement in sensitivity achievable is significantly less than the ideal value.

Recently, we had proposed an alternative protocol [11] using OATS that is somewhat similar to the CESP; in this paper we will refer to this as the generalized echo squeezing protocol (GESP), since it also employs inversion of the squeezing interaction. For a Ramsey clock, the basic steps of this protocol are similar to the ones described above for the CESP. However, there are several differences that, perhaps surprisingly, produce drastically different results. In order to point out the differences, it is important to note first that while the results of the CESP protocol does not depend on the parity of N , the results of the GESP protocol depend strongly on this parity in the interval $(\pi/2 - \sqrt{2/N}) \leq \mu \leq \pi/2$ (the range of μ of interest is from 0 to $\pi/2$ because the behavior of the system for values of μ from $\pi/2$ to π mirrors that for values of μ from 0 to $\pi/2$, and has an overall periodicity of π). Therefore, it is necessary to describe two versions of the GESP: one optimized for odd N in the interval $(\pi/2 - \sqrt{2/N}) \leq \mu \leq \pi/2$, and the other optimized for even N in that interval.

We denote as GESP-o (GESP-e) the version of the GESP optimized for odd (even) N . For the GESP-o, all the steps are the same as those for the CESP described above, with the exception that the last $\pi/2$ pulse rotation is around the y -axis. For GESP-e, the steps are similar to those used for the CESP, with the following differences. First, the auxiliary rotation after the OATS is carried out around the y -axis, and the reversal of the auxiliary rotation is also around the y -axis. Second, the last $\pi/2$ pulse rotation is around the y -axis. For both versions of the GESP, the signal measured is the expectation value of S_z , just as in the case of the CESP.

In reference [11], we had focused primarily on the investigation of the GESP-e protocol, emphasizing its behavior for the case when the squeezing parameter, μ , equals $\pi/2$. For this choice of the squeezing parameter, the system evolves into a maximally entangled Schrödinger cat state. Use of this protocol (the Schrödinger cat state protocol: SCSP) leads, ideally, to the maximum enhancement in sensitivity, to the Heisenberg limit. Furthermore, we showed that the mechanism for the enhancement in sensitivity is radically different from what is normally encountered in the use of OATS. Specifically, we showed that the fringes as a function of the phase is magnified by a factor of N , while the quantum projection noise (QPN) is also magnified by a factor of \sqrt{N} . We also showed that this magnification of the QPN makes this system extremely robust against excess noise. All these results can be proven analytically, for an arbitrarily large value of N . Nonetheless, we also carried out numerical simulations, for numerically accessible values of N , to demonstrate agreements with the analytical results. In the process of the numerical simulations, we also considered the behavior of the GESP-e protocol for the full range of the value of the squeezing parameter, μ , from 0 to $\pi/2$ (the behavior of the system for values of μ from $\pi/2$ to π mirrors that for values of μ from 0 to $\pi/2$, and has an overall periodicity of π). However, for values of μ less than $\pi/2$, the results we found and reported were based solely on numerical simulations, limited to relatively small values of N . As such, it was not clear what the general behavior of such a protocol would be for arbitrary values of N . Furthermore, the mechanism for the degree of enhancement was also not known. Specifically, we did not know whether the enhancement was accompanied by any enhancement in QPN. As such, we could not determine the degree of robustness of this protocol against excess noise for general values of the squeezing parameter.

Recently, we have developed analytical techniques that enable us to investigate the behavior of both types of GESP, for any value of μ and any value of N , with either parity. This enables us to compare the behavior of GESP with that of the CESP as well as the SCSP for the full range of parameters of interest. In the interval $0 \leq \mu \leq 1/\sqrt{N}$, the sensitivity of the GESP (for both versions) is close to the sensitivity of the CESP, and even exceeds that sensitivity for some values of μ . As μ increases from $1/\sqrt{N}$, the sensitivity of the CESP decreases to zero rapidly while that of the GESP (for both versions) keeps increasing, reaching the Heisenberg limit lowered by a factor of $\sqrt{2}$ at about $4\sqrt{2/N}$, and remains almost constant until $\mu = (\pi/2 - \sqrt{2/N})$. As μ increase from $(\pi/2 - \sqrt{2/N})$ to $\pi/2$, the sensitivity of the GESP goes to either the Heisenberg limit or the standard quantum limit depending on the combination of the version of the GESP and the parity of N , while the sensitivity of the CESP remains about zero. We also compare the sensitivity of the GESP and the CESP with their quantum Cramér-Rao bound (QCR bound). We find that for the GESP (both versions) the sensitivity remains very close to the QCR bound for the whole range of the squeezing parameter, while for the CESP the sensitivity is far below the QCR bound for values of the squeezing parameter beyond the one at which the peak sensitivity is achieved.

With the sensitivity analysis, we compare the mechanism of enhancement of sensitivity for the SCSP, the GESP and the CESP. In the case of the SCSP, the enhancement of sensitivity is due to an N -fold phase magnification, countered by a \sqrt{N} -fold enhancement in the quantum projection noise (QPN). In contrast, for the CESP, at its optimum point of operation, the enhancement is due only to a phase magnification by a factor of $\sim \sqrt{N/e}$, with no variation in the quantum noise. For the case of GESP, the mechanism depends on the value of the squeezing parameter. Consider

specifically the range of μ over which the enhancement of sensitivity remains essentially a constant, with a value of $\sim\sqrt{N/2}$. For small values of μ , the enhancement mechanism is similar to that of the CESP: it is due primarily to phase magnification by a factor of $\sim\sqrt{N/2}$, with no change in the QPN. For the values of μ close to $\pi/2$, the enhancement mechanism is similar to that of the SCSP: there is a phase magnification by a factor of $\sim N/2$, countered by an increase in the QPN by a factor of $\sim\sqrt{N/2}$. We note that the details of the mechanism of enhancement, while seemingly irrelevant, does in fact have great significance in the experimental context. As we showed in detail in reference [11], the extreme enhancement of the QPN in the case of the SCSP makes it very robust against the effect of excess noise. In fact, the protocol presented in reference [11] has been shown to achieve the maximum possible robustness against excess noise [12]. When the GESP is operated at the point where μ is close to $\pi/2$, it has a robustness against excess noise almost as high (within a factor of $\sqrt{2}$) as in the case of the SCSP. Furthermore, at this point, either version of the GESP works equally well for both parities of N . This makes the GESP a very attractive option experimentally. Furthermore, we also determine the shapes of the interference fringes for the SCSP, the GESP and the CESP to prove the phase magnification effect discussed above and to provide the expected results for the experiments measuring the interference fringes by scanning the phase shift.

The discussions presented above clearly show the potential advantages of using the GESP compared to the CESP experimentally. To summarize, for the GESP it is not necessary to tune the value of the squeezing parameter to a sharply peaked value. Furthermore, it can be operated in a regime where it is robust against the excess noise by a factor of $\sim\sqrt{N/2}$, while remaining insensitive to the parity of N . Finally, the GESP provides a general approach that bridges the

mechanism of the CESP with that of the SCSP, allowing for operation with the same enhancement of sensitivity, close to the Heisenberg limit, for an extremely broad range of values of μ .

The rest of the paper is organized as follows. We describe the GESP together with the SCSP and the CESP in Section 2, calculate the sensitivity of the GESP in Section 3, investigate the behavior of the sensitivity in Section 4, analyze the mechanism of the enhancement of sensitivity to show the robustness of the GESP in Section 5, analyze the fragility of all the protocols against collision with background atoms in Section 6, and present concluding remarks in Section 7.

2. Generalized echo squeezing protocol

We first review briefly the canonical two-level atom in order to establish the relevant notations used in this paper. A two-level atom is formally equivalent to a spin-1/2 spinor, with the spin operator represented as $\mathbf{s} = (s_x, s_y, s_z)$, where s_w ($w = x, y, z$) being the component of the spin operator in the w -direction. The two eigenstates of s_z are denoted as $|\uparrow\rangle$ and $|\downarrow\rangle$ with eigenvalues of $1/2$ and $(-1/2)$, respectively (setting $\hbar = 1$). The state of this atom can be described by a point on the Bloch sphere. A point on the Bloch sphere can be characterized by the polar and azimuthal angles, θ and ϕ , of a spherical coordinate system.

For an ensembles of N non-interacting atoms, the combined spin-operator is defined as:

$$\mathbf{S} \equiv (S_x, S_y, S_z) \equiv \sum_{j=1}^N \mathbf{s}_j \quad (1)$$

For such an ensemble, the j -th spinor in the state corresponding to such a point on the Bloch sphere is defined as [3] $|\langle \theta, \phi \rangle_j\rangle \equiv \cos(\theta/2)|\uparrow_j\rangle + e^{i\phi} \sin(\theta/2)|\downarrow_j\rangle$. A coherent spin state (CSS)

characterized by the angles θ and φ is defined as a state of N atoms with each atom in the state

$$\left|(\theta, \varphi)_j\right\rangle, \text{ that is } |\theta, \varphi\rangle \equiv \bigotimes_{j=1}^N \left|(\theta, \varphi)_j\right\rangle.$$

To describe the generalized echo squeezing protocol (GESp), we start by considering the limiting case where the squeezing parameter, μ , has the value of $\pi/2$. For this condition, the GESp is simply the Schrödinger cat state protocol (SCSP) [11]. We recall [11] that there are two types of SCSP, one optimized for even N (denoted as SCSP-e), while the other optimized for odd N (denoted as SCSP-o). The SCSP-e (SCSP-o) reaches the Heisenberg limit of sensitivity when N is even (odd) [13,14,15,16,17,18]. The steps in the SCSP-e, applied to a Ramsey atomic clock are as follows, illustrated schematically in Figure 1, using the Husimi quasi-probability distribution [3] for both even (top row) and odd (bottom row) values of N . First, a $\pi/2$ pulse around the y -axis is applied to the atoms in state $|\uparrow\rangle$ and turn the atoms into CSS $\left|\frac{\pi}{2}, 0\right\rangle$ (all pseudo-spinors in the x -direction). The effect of this step is equivalent to starting with atoms in CSS $\left|\frac{\pi}{2}, 0\right\rangle$. Then the atoms go through an OATS process with $\mu = \pi/2$, which produces a Schrödinger cat state oriented along the x -axis. Since the phase shift due to the detuning of the clock oscillator, denoted as ϕ , causes a rotation around the z -axis, an auxiliary pulse is applied to re-orient the Schrödinger cat state along the z -axis. This auxiliary rotation is then undone at the end of the dark period. As we show later in the paper, the combined processes of applying this auxiliary rotation, the accumulation of the phase shift around the z -axis, followed by reversing the auxiliary rotation, is equivalent to a rotation around the x -axis by the same angle ϕ . As such, for simplicity and brevity, we represent these three steps as a single step entailing a rotation around the x -axis. Next, the

atoms go through an inverse OATS process with $\mu = (-\pi/2)$. This is followed by another $\pi/2$ pulse around the y -axis, and the quantum operator that is measured is S_z . However, it can be shown that the combined effect of these two steps is equivalent to measuring the operator S_x . As such, for simplicity and brevity, we represent these two steps as a single one representing measurement of S_x . As can be seen by comparing the top row with the bottom one, the evolution of the quantum states during various stages of the protocol for even N differ significantly from those generated for odd N . This difference between the two parities of N is due to the fact that the Schrödinger cat state generated by the first OATS process is x -directed (top row) for even N but y -directed (bottom row) for odd N .

In Figure 2, we illustrate the corresponding steps for the SCSP-o, with the top (bottom) row corresponding to even (odd) values of N . The first two steps are the same as those for the SCSP-e. However, since the Schrödinger cat generated after the application of the OATS pulse is oriented around the y -axis, the auxiliary rotation used for aligning them along the z -axis and inversion thereof at the end of the dark zone occurs around the x -axis. As we also show later in this paper, the combined effect of the processes of the auxiliary rotation, the rotation around the z -axis by the angle ϕ , and reversing the auxiliary rotation, is a rotation around the y -axis by the same angle ϕ , as indicated here. The remainder of the protocol is identical to that of the SCSP-e. Therefore, we see that the SCSP-o differs from the SCSP-e only in the fact that the rotation representing the phase shift occurs around the y -axis (in practice, this represents a difference in the axis around which the auxiliary rotation is applied and undone later on). Again, we see that the evolution of the quantum states depends significantly on the parity of N , for the same reason as the one described above for SCSP-e.

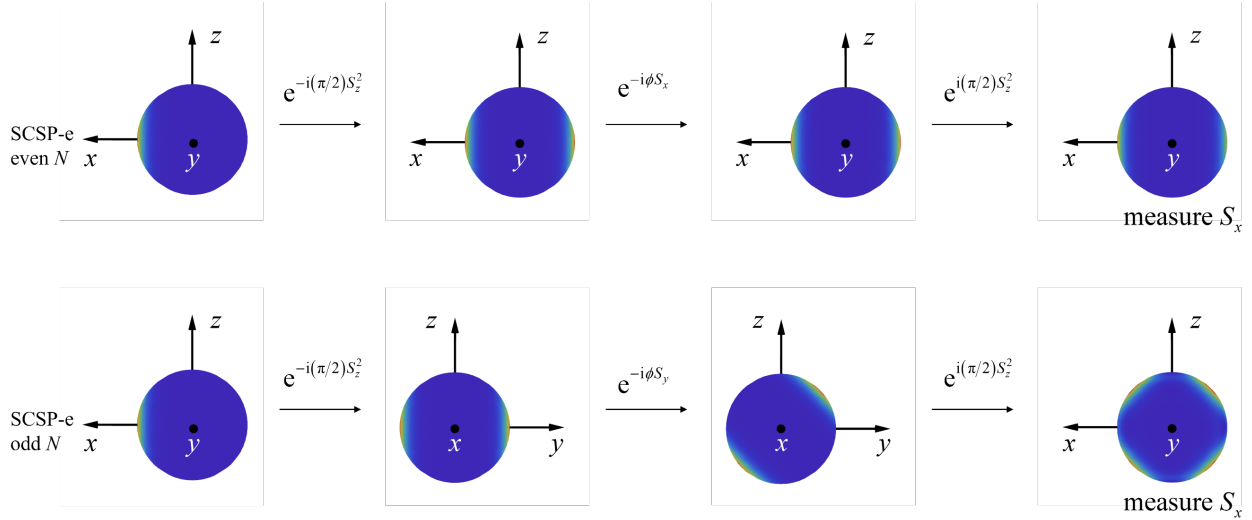


Figure 1. Steps of the Schrödinger cat state protocol optimized for even N (SCSP-e) and the state evolution for even N (top row) and odd N (bottom row) demonstrated by the Husimi quasi-probability distribution. The atoms prepared in the CSS $\left|\frac{\pi}{2}, 0\right\rangle$ (all pseudo-spinors in the x -direction) first go through the OATS process with $\mu = \pi/2$, then accumulate phase shift due to the detuning of the clock oscillator to the clock transition, denoted as ϕ . Here, we have made use of the fact that the effective rotation due the phase shift occurs around the x -axis, as explained in detail in the body of the paper. Finally, the atoms go through an inverse OATS process with $\mu = (-\pi/2)$. The effective quantum operator we measure in the end is S_x , as also explained in the body of the paper. As can be seen by comparing the top row with the bottom one, the quantum states generated for even N differ significantly from those generated for odd N .

The two types of generalized echo squeezing protocols, namely GESP-e and GESP-o, are simply generalized versions of the SCSP-e and SCSP-o described above, for an arbitrary value of the squeezing parameter, μ . In the top two rows of Figure 3, we illustrate the behavior of the GESP-e and GESP-o, respectively, for $N = 40$ and $\mu = \text{arccot} \sqrt{N-2} \approx 1/\sqrt{N}$. This value of μ is chosen because it gives the optimal enhancement of sensitivity of the CESP [1]. To compare the behavior of the quantum states under the two versions of the GESP with that of the CESP, this value of μ is used for all these protocols. As we will show later, the behavior of the quantum states under either version of the GESP generally does *not* depend on the parity of N , until the

value of μ gets very close to $\pi/2$, and this condition is satisfied for the plots shown in the top two rows.

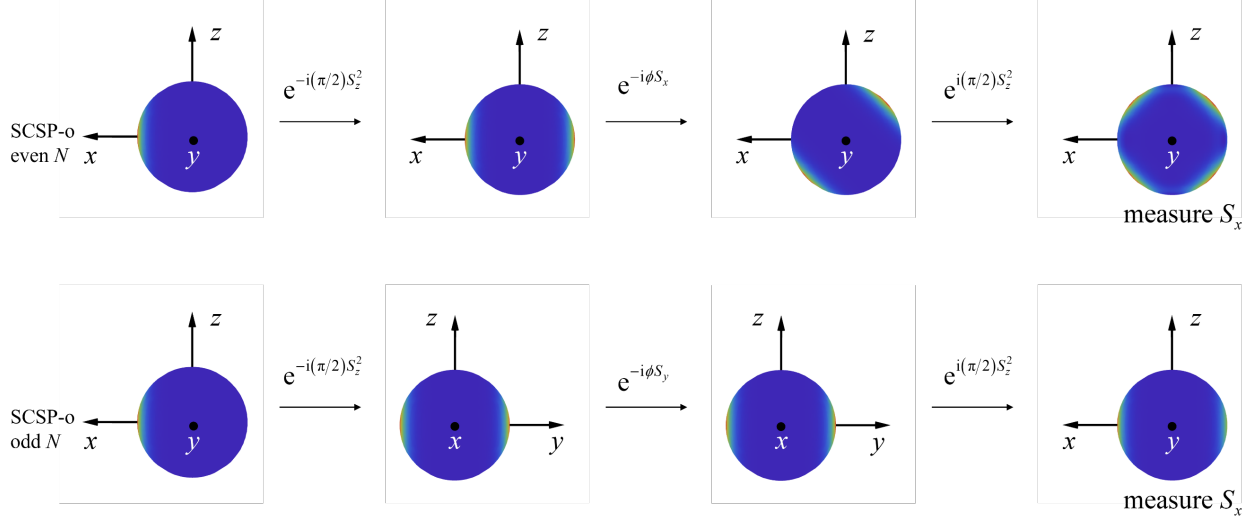


Figure 2. Steps of the Schrödinger cat state protocol optimized for odd N (SCSP-o) and the state evolution for even N (top row) and odd N (bottom row) demonstrated by the Husimi quasi-probability distribution. It differs from the SCSP-e process (as illustrated in Figure 1) only in the fact that the effective phase shift induced rotation occurs around the y -axis. Again, as can be seen by comparing the top row with the bottom one, the quantum states generated for odd N differ significantly from those generated for even N .

In the bottom row of Figure 3, we illustrate the steps employed in the CESP. Here, we have again used to approach where an equivalent simple rotation around an axis is used to represent the combined effect of multiple steps that would be required experimentally. In order to see clearly the similarities and difference between the CESP and the two versions of the GESP, it is instructive to look instead at the actual steps necessary to realize the CESP experimentally for an atomic clock, as illustrated in Figure 4, for the value of μ that yields the optimal enhancement in sensitivity. Just as in the case of each version of the GESP protocol, the process starts with the application of a $\pi/2$ pulse around the y -axis to the atoms in state $|\uparrow\rangle$, to produce the CSS $\left|\frac{\pi}{2}, 0\right\rangle$. The effect of

this step is equivalent to starting with the atoms in the CSS $\left| \frac{\pi}{2}, 0 \right\rangle$. The atoms then go through an OATS process with $\mu = \text{arccot} \sqrt{N-2} \approx 1/\sqrt{N}$. This is followed in sequence by three steps: an auxiliary rotation around the x -axis, the rotation around the z -axis by an angle of ϕ due to the phase shift, and the reversal of the auxiliary rotation. These three steps are equivalent to a rotation around the y -axis by an angle of ϕ (as shown in the bottom row of Figure 3). Next, the atoms go through an inverse OATS process. The net result of these additional four steps (namely, squeezing, auxiliary rotation, inversion of auxiliary rotation, and inverse squeezing) is a CSS state that would have been produced if the rotation around the z -axis were equal to a $\sim \phi\sqrt{N/e}$ (for small ϕ) without applying the additional four steps. As such, the net effect of the process is a phase magnification by a factor of $\sim \sqrt{N/e}$ [19]. To measure this rotation around the z -axis, the CESP protocol uses a $\pi/2$ pulse around the x -axis, followed by a measurement of S_z [20]. Measuring S_z after the last $\pi/2$ pulse around the x -axis is equivalent to measuring S_y (as shown in the bottom row of Figure 3.) It should be noted that the rotation axis of this last $\pi/2$ pulse is different from that of the first $\pi/2$ pulse, in contrast to the conventional Ramsey protocol, the SCSP, and the GESP.

We now refer back to the equivalent and simplified representations of the protocols as summarized in Figure 3. As can be seen, the CESP differs significantly from the GESP-e, but is very similar to the GESP-o. They are identical except only the quantum operator we measure in the end. In the GESP-o, we measure S_x while in the CESP we measure S_y . When considering the actual steps involved in these protocols, the actual difference between the GESP-o the CESP is the rotation axis of the last $\pi/2$ pulse before detection.

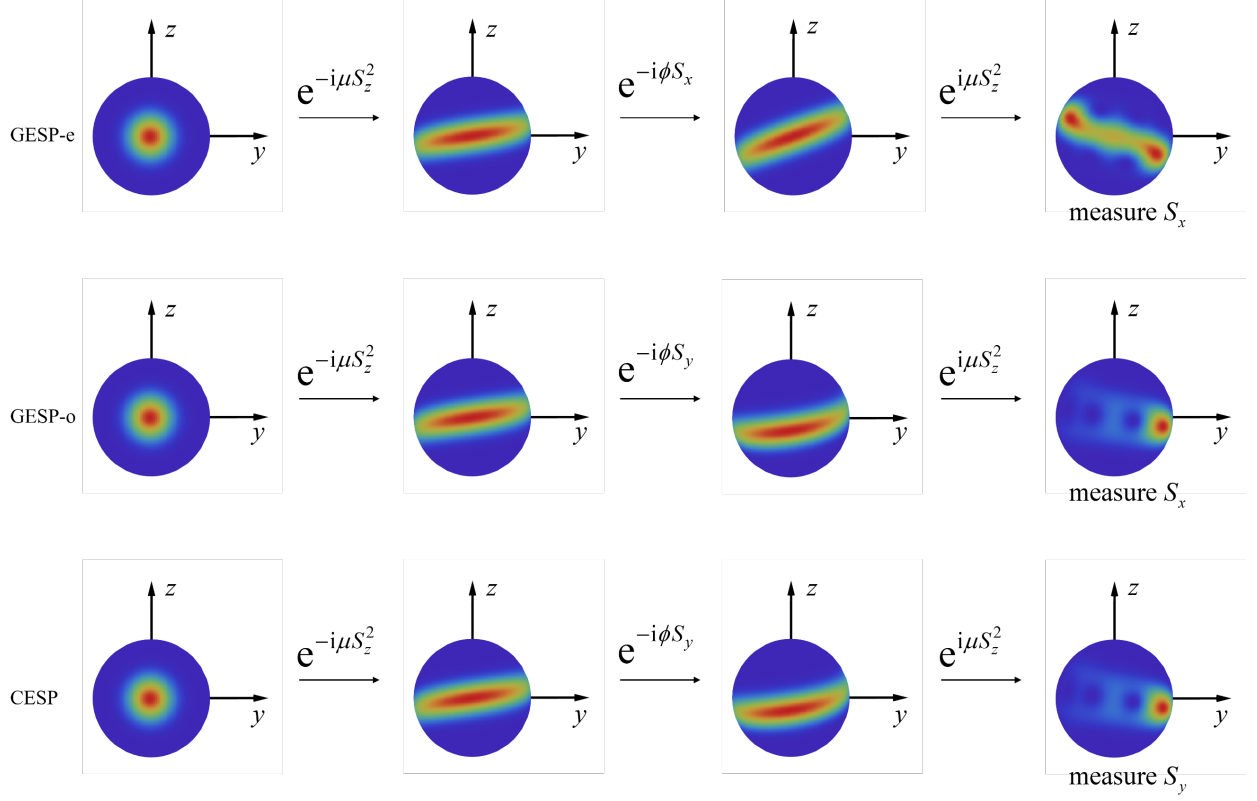


Figure 3. Generalized echo squeezing protocol GESP-e and GESP-o and the conventional echo squeezing protocol (CESP). See text for details.

In the preceding discussions, we have extensively made use of the fact that multiple steps in the spin squeezing protocols can be combined into a single, effective step. Before proceeding further, we present first the mathematical analysis underlying this process. We note first the following relations:

$$f\left(\begin{matrix} S_x \\ y \end{matrix}\right) = R_y\left(\pm\frac{\pi}{2}\right)f(S_z)R_x\left(\mp\frac{\pi}{2}\right) \quad (2)$$

where f is an arbitrary analytical function, and the rotational operator is defined as, for example, $R_x(\alpha) \equiv e^{-i\alpha S_x}$. In Eq. (2), the upper and lower subscripts correspond to the upper and lower signs, respectively, for the rotation operations; the same convention is used throughout the rest of the

paper. For the GESF applied to the Ramsey atomic clock, we write the rotational operator describing the detuning induced phase shift, using Eq. (2), as

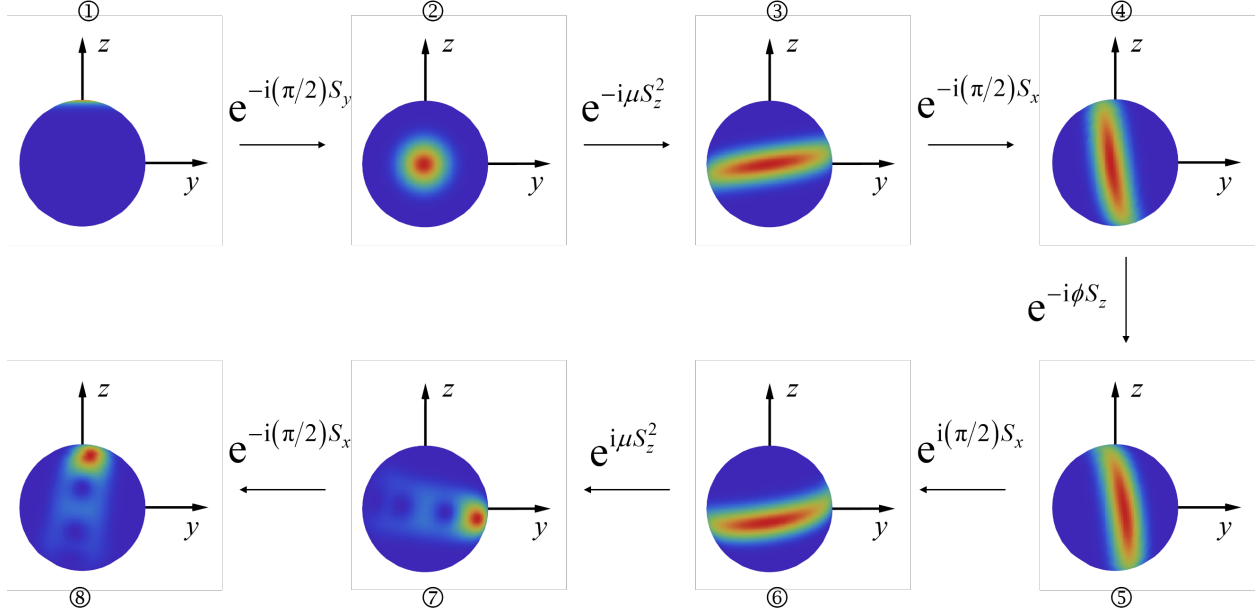


Figure 4. Complete conventional echo squeezing protocol (CESP) for the atomic clock. See text for details.

$$R_{y/x}(\phi) = R_{y/x}\left(\pm\frac{\pi}{2}\right)R_z(\phi)R_{y/x}\left(\mp\frac{\pi}{2}\right) \quad (3)$$

From Eq. (3), we can see that just by sandwiching the dark period phase evolution (which is always assumed to occur physically around the z -axis) between the auxiliary rotation and the inverse auxiliary rotation, we can model the phase shift as a single rotation around either the x -axis or the y -axis. Normally, the quantum operator we measure is S_z . This is equivalent to measuring S_x if

we add a $\pi/2$ pulse $R_{y/x}(\mp\pi/2)$ before the detection process. This can be seen by noting that,

according to Eq. (2), $S_{y/x} = R_{y/x}(\pm\pi/2)S_zR_{y/x}(\mp\pi/2)$, so that:

$$\langle \psi | S_y | \psi \rangle = \langle \psi | R_x \left(\pm \frac{\pi}{2} \right) S_z R_x \left(\mp \frac{\pi}{2} \right) | \psi \rangle \quad (4)$$

It should be noted that there could be many equivalent variants of the simplified versions of the protocols because flipping the sign of the rotation angle of a $\pi/2$ pulse (for example, changing $R_y(-\pi/2)$ to $R_y(\pi/2)$) will only result in an additional minus sign in the final signal (this applies to all $\pi/2$ pulses, including the auxiliary pulse and its inverse). If we flip the signs of the rotation angles of two $\pi/2$ pulses, then the two minus signs in front of the final signal cancel out and the final signal will not be changed. Therefore, in practice, for all the $\pi/2$ pulses (including the auxiliary pulse and its inverse), we only need to specify the rotation axis, but do not need to care whether it is a clockwise or counterclockwise rotation.

For concreteness, the protocols have so far been illustrated only in the context of the Ramsey atomic clock above. With proper modifications, these protocols can also be applied to the light pulse atom interferometer (LPAI). Here, we show in detail how to adapt these protocols to the LPAI [21,22,23]. Recalling briefly, the conventional LPAI works as follows. The process starts with the pseudo-spins of all atoms pointing in the $+z$ -direction. The wave packet of each atom is then split into two components by using a $\pi/2$ pulse of a pair of counter-propagating Raman beams. This step is formally equivalent to the application of a $\pi/2$ pulse in a Ramsey atomic clock. Each of the two components have different transverse momentum; as a result, the wave packet of the atoms gets spatially separated. After a dark period T , the two components interact again with the Raman beams, corresponding to a π pulse. After another dark period of T , another $\pi/2$ pulse is applied. This is followed by the detection of S_z . The phase shift in the LPAI can be due to various effect; for concreteness, we consider here the case where the phase shift is due to the Sagnac effect [24]. Furthermore, we assume that half of the phase accumulation occurs before the

π pulse, while the remaining half occurs after the π pulse. Noting that $R_y(\pi) = R_y(-\pi)$, the propagator describing the conventional LPAI protocol can be expressed as

$$\begin{aligned}
& R_y\left(\frac{\pi}{2}\right)R_z\left(-\frac{\phi}{2}\right)R_y(-\pi)R_z\left(\frac{\phi}{2}\right)R_y\left(\frac{\pi}{2}\right) \\
&= \left[R_y\left(\frac{\pi}{2}\right)R_z\left(-\frac{\phi}{2}\right)R_y\left(-\frac{\pi}{2}\right) \right] \left[R_y\left(-\frac{\pi}{2}\right)R_z\left(\frac{\phi}{2}\right)R_y\left(\frac{\pi}{2}\right) \right] \\
&= R_x\left(-\frac{\phi}{2}\right)R_x\left(-\frac{\phi}{2}\right) = R_x(-\phi)
\end{aligned} \tag{5}$$

The first line in this equation expresses the propagator in a manner that corresponds to the actual physical steps. In going from the second line to the third line, we have made use of the rules stated in Eq. (3). Thus, we see that the whole LPAI operation can be viewed simply as a rotation around the x -axis by an angle of $(-\phi)$. Noting that the equivalent step for the conventional Ramsey atomic clock is also $R_y(-\pi/2)R_z(\phi)R_y(\pi/2) = R_x(-\phi)$ (here, we have made use of the fact that the sign of the rotation angle of any $\pi/2$ pulse does not affect the observable signal, as noted earlier), we can see that the single equivalent step of the conventional Ramsey clock is identical to that of the LPAI.

When the squeezing process is introduced, thus creating entangled states of the atoms, it may not be a priori clear how to account for the Sagnac effect in the LPAI. To address this issue, we reconsider first the case of the conventional LPAI in which the atoms are not entangled. In this case, we can simply consider each atom separately. The one-atom state $|\uparrow\rangle$ and $|\downarrow\rangle$ both have well-defined trajectories, which will form a well-defined enclosed area. Therefore, it is obvious that the Sagnac phase shift gained by one atom is $\phi = 2m\boldsymbol{\Omega} \cdot \boldsymbol{A}$ (still setting $\hbar = 1$) where m is the mass of one atom, $\boldsymbol{\Omega}$ is the rotational velocity of the LPAI, and \boldsymbol{A} is the vectorial area enclosed

by the two arms of the LPAI [24]. Accordingly, as we have done in Eq. (5), the Sagnac phase shift can be described by the propagator $e^{-i(\phi/2)S_z}$ in the first dark period and $e^{i(\phi/2)S_z}$ in the second dark period (the change in sign is due to the π pulse in the middle). For the case where atoms are entangled, we consider first the simplest case, namely the z-directed Schrödinger cat state generated, for example, in the SCSP-e protocol for even N applied to the LPAI [24]. In this case, there are only two quantum states (all atoms in state $|\uparrow\rangle$ and all atoms in state $|\downarrow\rangle$) each with a well-defined trajectory. Consequently, the Sagnac phase shift for the whole ensemble is simply $N\phi$, because the mass of each quantum state is Nm [24]. This Sagnac phase shift still can be described by the propagator $e^{-i(\phi/2)S_z}$ in the first dark period and $e^{i(\phi/2)S_z}$ in the second dark period. This is affirmed by noting that the resulting effect agrees with the physical interpretation of the phase magnification stated above.

Consider next the case where the quantum state produced after the first squeezing pulse is not a simple Schrödinger cat state, but rather an arbitrary superposition of the symmetric Dicke states [25,26]. We recall that such a Dicke state is a superposition of many direct product states. A direct product state is an N -atom state where each atom is either in state $|\uparrow\rangle$ or $|\downarrow\rangle$ but not a superposition. For such a direct product state, each atom has a well-defined trajectory. However, a direct product state as a whole does not have a well-defined trajectory because some atoms are in state $|\uparrow\rangle$ and follow one arm while the other atoms are in state $|\downarrow\rangle$ and follow the other arm. In this case, we must consider the Sagnac phase shift contributed by each atom. In a Dicke state (with the exception of the extremal ones), the atoms are entangled. Nonetheless, it is still true that for each atom, state $|\uparrow\rangle$ and $|\downarrow\rangle$ will follow the two arms of the LPAI and gain different phases, whose difference is the overall Sagnac phase shift for the atom. This effect, for each atom, can still

be described by the propagator $e^{-i(\phi/2)S_z}$ (noting that s_z here is in lowercase, meaning the single atom operator) in the first dark period and $e^{i(\phi/2)S_z}$ in the second dark period. The Sagnac phase shift for the whole ensemble can then be described by the direct product of these single-atom propagators, namely $e^{-i(\phi/2)S_z}$ in the first dark period and $e^{i(\phi/2)S_z}$ in the second dark period; this follows from the definition of S_z in Eq. (1). Not surprisingly, this formulation yields the correct result for the unentangled atoms as well for the case of the z -directed Schrödinger cat state.

The complete protocol of the GESP-e(o) for the LPAI can now be expressed as follows [24]: $\pi/2$ pulse around the y -axis applied to atoms in state $|\uparrow\rangle$, squeezing, auxiliary rotation around the $y(x)$ -axis, the first dark period, π pulse around the $y(x)$ -axis, the second dark period, the inverse auxiliary rotation, the inverse squeezing process, and a $\pi/2$ pulse around the y -axis. The final state expressed in terms of the propagator of the GESP-e(o) steps is shown in Eq. (6), where $|\uparrow\rangle$ denotes the CSS with all the atoms in state $|\uparrow\rangle$.

$$|\psi_e\rangle = R_y\left(\frac{\pi}{2}\right)e^{i\mu S_z^2}R_x\left(\mp\frac{\pi}{2}\right)R_z\left(-\frac{\phi}{2}\right)R_x(\pi)R_z\left(\frac{\phi}{2}\right)R_x\left(\mp\frac{\pi}{2}\right)e^{-i\mu S_z^2}R_y\left(\frac{\pi}{2}\right)|\uparrow\rangle \quad (6)$$

For $\mu = \pi/2$, Eq. (6) reproduces the result reported previously in Refs. [11] and [24] for the SCP protocols.

Ref. [1] does not explicitly consider the adaptation of the CESP protocol to the LPAI. However, following the same logic that was used for the CESP protocol for the Ramsey atomic clock, we can easily see that the CESP for the LPAI would be essentially identical to the GESP-o, with the only difference being that the last $\pi/2$ pulse is around the x -axis. Of course, just in the case of the Ramsey clock, CESP-e differs significantly from the GESP-e. It should be noted that

the middle π pulse in the GESP-o and the CESP is around the x -axis, in contrast to the conventional LPAI and the GESP-e.

The middle five steps for any of these protocols (the auxiliary rotation, the first dark period, π pulse, the second dark period, the inverse auxiliary rotation) is equivalent to a single rotation around the x - or y -axis, according to the relations

$$R_{y,x}(\phi) = R_{y,x}\left(\mp \frac{\pi}{2}\right) R_z\left(-\frac{\phi}{2}\right) R_{y,x}(\pi) R_z\left(\frac{\phi}{2}\right) R_{y,x}\left(\mp \frac{\pi}{2}\right) \quad (7)$$

It is now obvious that these complete protocols for the LPAI employing spin-squeezing are equivalent to the corresponding ones for the Ramsey atomic clock employing spin-squeezing shown earlier in Figure 3. As discussed above, for all the $\pi/2$ pulses (including the auxiliary pulse as well as its inverse), we only need to care about the rotation axis, but do not need to care about the sign of the rotation angle. Furthermore, obviously a π pulse is always equivalent to a $(-\pi)$ -pulse around the same axis. Therefore, for any protocol, either for the Ramsey atomic clock or the LPAI, the sign of the rotation angle can be flipped for any of the pulses.

3. Sensitivity and the quantum Cramér-Rao bound of the GESP and the CESP

For both the Ramsey clock and the light pulse atom interferometer, the fundamental uncertainty in the measurement is directly proportional to uncertainty in the measurement of the phase shift accumulated during the interaction. As such, the sensitivity of a protocol is characterized by the reciprocal of minimum measurable change in the phase, denoted as $\Delta\phi^{-1}$. The goal of any spin squeezing protocol is to maximize this parameter, which can be expressed in general as:

$\Delta\phi^{-1}\big|_{\phi=0} = \left(\left| \partial_\phi \langle S_w \rangle \right| / \Delta S_w \right)_{\phi=0}$, where S_w is the spin operator we measure, and ΔS_w is the standard deviation. The sensitivity of the CESP, considering only the quantum projection noise, has been analytically calculated [1] to be $\Delta\phi^{-1}\big|_{\phi=0} = \sqrt{2S} (2S-1) \cos^{2S-2} \mu \sin \mu$, with $S = N/2$, while the sensitivity of the GESP has only been investigated with numerical simulation [11,24]. The numerical simulation is constrained by three limitations. First, it is very difficult to simulate the result for very large values of N . Second, little insight can be gained from the behavior determined for a limited range of values of N . Third, the actual mechanism underlying the enhancement of sensitivity, as an interplay between different degrees of phase magnification and enhancement of the quantum projection noise, is not at all evident. To overcome these constraints, we have developed analytic expressions for determining the sensitivity of the GESP, as described next.

The final state of the three-step GESP shown in Figure 3 is

$$\left| \psi_{\circ} \right\rangle = e^{i\mu S_z^2} e^{-i\phi S_y} e^{-i\mu S_z^2} \left| \frac{\pi}{2}, 0 \right\rangle = e^{i\mu S_z^2} \left(1 - i\phi S_y - \frac{1}{2}\phi^2 S_y^2 + \mathcal{O}(\phi^3) \right) e^{-i\mu S_z^2} \left| \frac{\pi}{2}, 0 \right\rangle \quad (8)$$

The corresponding signal is then given by:

$$\begin{aligned} \left\langle \psi_{\circ} \left| S_x \right| \psi_{\circ} \right\rangle &= \langle S_x \rangle - i\phi \left\langle \left[S_x, \tilde{S}_y \right] \right\rangle + \phi^2 \left\langle \left(\tilde{S}_y S_x \tilde{S}_y - \frac{1}{2} \{ S_x, \tilde{S}_y^2 \} \right) \right\rangle + \mathcal{O}(\phi^3) \\ &= S + \phi^2 \left\langle \left(\tilde{S}_y S_x \tilde{S}_y - \frac{1}{2} \{ S_x, \tilde{S}_y^2 \} \right) \right\rangle + \mathcal{O}(\phi^4) \\ &= S + \phi^2 \left(\left\langle \tilde{S}_y S_x \tilde{S}_y \right\rangle - S \left\langle \tilde{S}_y^2 \right\rangle \right) + \mathcal{O}(\phi^4) \end{aligned} \quad (9)$$

where, we define, for example, $\left\langle S_x \right\rangle \equiv \left\langle \frac{\pi}{2}, 0 \left| S_x \right| \frac{\pi}{2}, 0 \right\rangle$ and $\tilde{S}_x \equiv e^{i\mu S_x^2} S_x e^{-i\mu S_x^2}$. The two steps in Eq. (9) are both based on the fact that the CSS $\left| \frac{\pi}{2}, 0 \right\rangle$ is an eigenstate of S_x with the eigenvalue of $S = N/2$. Here, the linear term proportional to ϕ vanishes as expected because the signal of the GESP is symmetric about $\phi = 0$. In fact, all odd order terms of ϕ vanish for the same reason. Therefore, in Eq. (9), the residual term in the second line becomes $\mathcal{O}(\phi^4)$. The details of the calculation of the signal are presented in Appendix. The result is:

$$\left\langle \psi_{\circ} \left| S_x \right| \psi_{\circ} \right\rangle = S + \phi^2 (\mathbf{a}_{10} \cdot \mathbf{b}_0 \pm \mathbf{a}_{11} \cdot \mathbf{b}_1) + \mathcal{O}(\phi^4) \quad (10)$$

where the expressions of the vectors \mathbf{a}_{10} , \mathbf{a}_{11} , \mathbf{b}_0 , and \mathbf{b}_1 are given in Appendix. Applying the same approach as outlined above for deriving the signal, we find the standard deviation to be:

$$\Delta S_x^2 \equiv \left\langle \psi_{\circ} \left| S_x^2 \right| \psi_{\circ} \right\rangle - \left\langle \psi_{\circ} \left| S_x \right| \psi_{\circ} \right\rangle^2 = \phi^2 S^4 (\mathbf{a}_{30} \cdot \mathbf{b}_0 \pm \mathbf{a}_{31} \cdot \mathbf{b}_1) + \mathcal{O}(\phi^4) \quad (11)$$

The detail of steps in the derivation of this result as well as the expressions for the vectors \mathbf{a}_{30} and \mathbf{a}_{31} are also shown in Appendix.

If we substitute Eqs. (10) and (11) into $\Delta \phi_{\circ}^{-1} \Big|_{\phi=0} = \left(\left| \partial_{\phi} \left\langle S_x \right\rangle \right| / \Delta S_x \right) \Big|_{\phi=0}$, we find that both

the numerator and the denominator are zero. Therefore, we calculate the sensitivity by applying the L'Hôpital's rule:

$$\Delta \phi_{\circ}^{-1} \Big|_{\phi=0} = \lim_{\phi \rightarrow 0} \frac{\left| \partial_{\phi} \left\langle S_x \right\rangle \right|}{\Delta S_x} = \frac{\partial_{\phi} \left| \partial_{\phi} \left\langle S_x \right\rangle \right|}{\partial_{\phi} \Delta S_x} \Big|_{\phi=0} = \frac{2 |\mathbf{a}_{10} \cdot \mathbf{b}_0 \pm \mathbf{a}_{11} \cdot \mathbf{b}_1|}{\sqrt{\mathbf{a}_{30} \cdot \mathbf{b}_0 \pm \mathbf{a}_{31} \cdot \mathbf{b}_1}} \quad (12)$$

The quantum Cramer-Rao (QCR) bound determines the maximum sensitivity that can be achieved, thereby representing the optimal retrieval of the quantum Fisher information present in the system

[27]. For a pure state, the QCR bound for phase sensitivity is given by $\Delta \phi_{\circ}^{-1} \Big|_{\phi=0} \leq 2 \Delta S_{\hat{n}}$, where

$\hat{\mathbf{n}}$ is the axis of the rotation representing the phase shift, $\mathcal{S}_{\hat{\mathbf{n}}} \equiv \mathcal{S} \cdot \hat{\mathbf{n}}$, and $\Delta S_{\hat{\mathbf{n}}}$ is the standard deviation of $S_{\hat{\mathbf{n}}}$ for the state just before introducing the phase shift. Using the result of the standard deviation after one-axis-twist squeezing process shown in Ref. [3], we can write the QCR bound for the GESP-e as

$$\Delta\phi^{-1}\Big|_{\phi=0} \leq 2\Delta S_x = \sqrt{2S\left(S + \frac{1}{2}\right) + 2S\left(S - \frac{1}{2}\right)\cos^{2S-2} 2\mu - \left(2S\cos^{2S-1} \mu\right)^2} \quad (13)$$

and the QCR bound for the GESP-o and CESP as

$$\Delta\phi^{-1}\Big|_{\phi=0} \leq 2\Delta S_y = \sqrt{2S\left(S + \frac{1}{2}\right) - 2S\left(S - \frac{1}{2}\right)\cos^{2S-2} 2\mu} \quad (14)$$

The sensitivity and the QRC bound of the GESP-e, GESP-o, and the CESP for $N = 100$ and 101 are plotted in Figure 5. In each case, it can be seen that the sensitivity of the GESP is close to the QRC bound over the whole range of μ , while the sensitivity of the CESP is close to the QRC bound in a small interval of μ near zero. These behaviors of the sensitivities mean that the CESP wastes almost all quantum Fisher information except in the proximity of $\mu = 0$, while both versions of the GESP makes good use of the quantum Fisher information. Other advantages of the GESP will be discussed in Section 4.

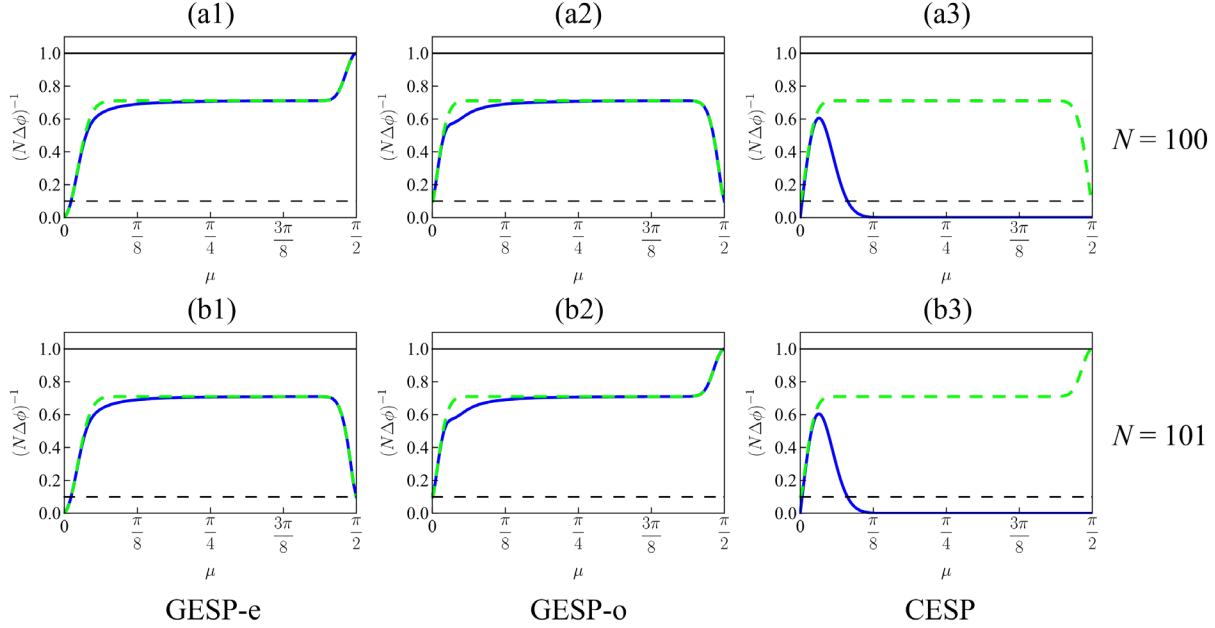


Figure 5. Sensitivity (blue solid) and the quantum Cramér-Rao bound (green dashed) of (a1)(b1) the GESP-e, (a2)(b2) the GESP-o, and (a3)(b3) the CESP for (a1)(a2)(a3) $N = 100$ and (b1)(b2)(b3) $N = 101$, normalized to the Heisenberg limit. The solid black line is the Heisenberg limit, and the dashed black line is the standard quantum limit.

4. Properties of the sensitivity of the GESP

It can be seen from Figure 5 that the sensitivity of the GESP, as expressed in Eq. (12), first increases as μ increases from 0, and remains almost a constant until μ approaches $\pi/2$, and then either increases to the Heisenberg limit or decreases to the standard quantum limit depending on the pairing of the parity of N and the protocol as discussed in Section 2. While it may not be apparent from Eq. (12), it turns out that the behavior, as a function of the squeezing parameter μ , of the quantity $\cos^{2S}(2\mu)$ plays a key role in determining how the sensitivity varies as a function of μ . To see why this is the case, note first that the expression for the sensitivity (namely Eq. (12)) depends on six vectors. Of these, only the vectors \mathbf{b}_0 and \mathbf{b}_1 depend on the squeezing parameter μ , as can be seen in Appendix. The vector \mathbf{b}_0 depends only on small powers of

$\cos(2\mu)$, while the vector \mathbf{b}_1 depends on very large powers of $\cos(2\mu)$ for large values of $N = 2S$. It is easy to see that in this limit (i.e, for a large value of N), the function $\cos^{2S}(2\mu)$ decreases from 1 to ~ 0 quickly as μ increases from 0, and remains ~ 0 until μ approaches $\pi/2$. As μ approaches $\pi/2$, the function $\cos^{2S}(2\mu)$ increases to 1 if N is even, and decreases to (-1) if N is odd. This is why the sensitivity for the values of μ close to $\pi/2$ highly depends on the parity of N . The function $\cos^{2S}(2\mu)$ is plotted in Figure 6 for $N = 100$ (solid blue) and $N = 101$ (dashed red). Now we estimate the interval of μ over which $\cos^{2S}(2\mu)$ is ~ 0 . Here, for computational convenience, we assume that $\cos^{2S}(2\mu)$ is ~ 0 if its absolute value is less than $e^{-4} \approx 0.018$. Solving the inequality $\cos^{2S}(2\mu) \leq e^{-4}$, we find this range to be $S^{-1/2} \leq \mu \leq (\pi/2 - S^{-1/2})$ for $S \gg 1$. Over this interval, we can substitute $\cos^{2S}(2\mu)$ with 0 in Eq. (12), which yields:

$$\begin{aligned} \Delta\phi_{\circ}^{-1} \Big|_{\phi=0} &\approx \frac{2(\mathbf{a}_{10} \cdot \mathbf{b}_0)}{\sqrt{\mathbf{a}_{30} \cdot \mathbf{b}_0}} \\ &= \frac{\sqrt{2S} \left[(1 - \cos 2\mu) + S^{-1} \frac{1}{2} (1 - \cos 2\mu) + S^{-2} \frac{1}{2} \cos 2\mu \right]}{\sqrt{(1 - \cos 2\mu)^2 + S^{-1} (1 - \cos 2\mu) + S^{-2} \left(\frac{3}{4} + \cos 2\mu - \frac{7}{4} \cos^2 2\mu \right) - S^{-3} \frac{1}{4} (1 - 3 \cos^2 2\mu)}} \end{aligned} \quad (15)$$

If the condition that $(1 - \cos 2\mu)^2 \gg S^{-1} (1 - \cos 2\mu)$ is satisfied, this expression can be further simplified to give:

$$\Delta\phi_{\circ}^{-1} \Big|_{\phi=0} \approx \frac{\sqrt{2S} (1 - \cos 2\mu)}{\sqrt{(1 - \cos 2\mu)^2}} = \sqrt{2S} = \frac{N}{\sqrt{2}} \quad (16)$$

The result of Eq. (16) is a sensitivity that is within a factor of $\sqrt{2}$ of the Heisenberg limit.

To establish a clearer, albeit approximate, meaning of the condition used in generating Eq. (16), we again make a computationally convenient specification that the condition $(1 - \cos 2\mu)^2 \gg S^{-1}(1 - \cos 2\mu)$ is satisfied if $(1 - \cos 2\mu)^2 \geq 32S^{-1}(1 - \cos 2\mu)$, which in turn implies that $(1 - \cos 2\mu) \geq 32S^{-1}$. It is easy to see from this inequality that for a very large value of S , the value of 2μ has to be very small, so that we can expand $\cos(2\mu)$ to second order in μ around $\mu = 0$. We then get the simple expression that $\mu \geq 4S^{-1/2}$. Combining this with the range of validity established in producing Eq. (15), we thus get the result that for $4S^{-1/2} \leq \mu \leq (\pi/2 - S^{-1/2})$, the sensitivity of the GESP is approximately $N/\sqrt{2}$. It can be shown that this range agrees closely with exact evaluations of the sensitivity using Eq. (12). This property of the sensitivity of the GESP means that for large N , we can work at almost any value of μ except for a narrow intervals near $\mu = 0$ and $\mu = \pi/2$, to obtain a sensitivity that is within a factor of $\sqrt{2}$ of the Heisenberg limit, as shown in Figure 7. On the contrary, the peak of the sensitivity curve of the CESP becomes very narrow for a large N . The sensitivity of the CESP becomes ~ 0 when $\cos^{2S}(\mu) \approx 0$ according to its analytical expression shown earlier. This means that the sensitivity of the CESP is greater than 0 only in the interval $0 < \mu < 2S^{-1/2}$. Therefore, when using the CESP, one must tune the value of μ very precisely in an experiment to obtain an enhancement of the sensitivity.

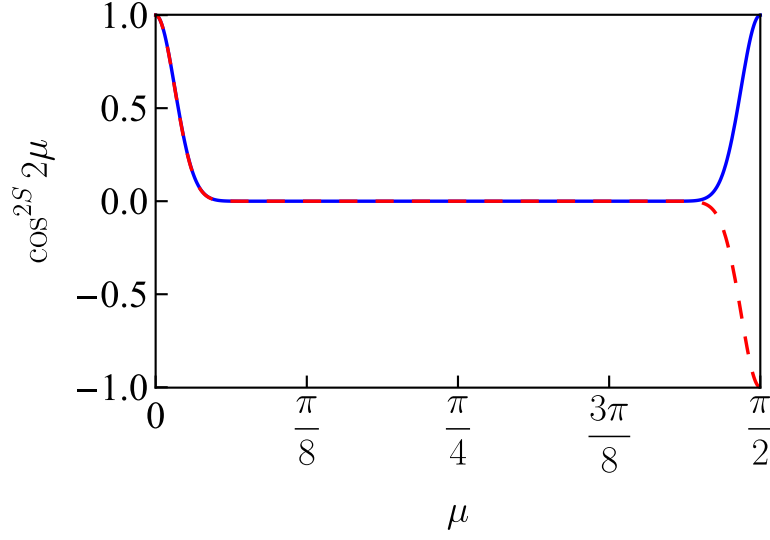


Figure 6. Plot of $\cos^{2S} 2\mu$ for $N=100$ (solid blue) and $N=101$ (dashed red).

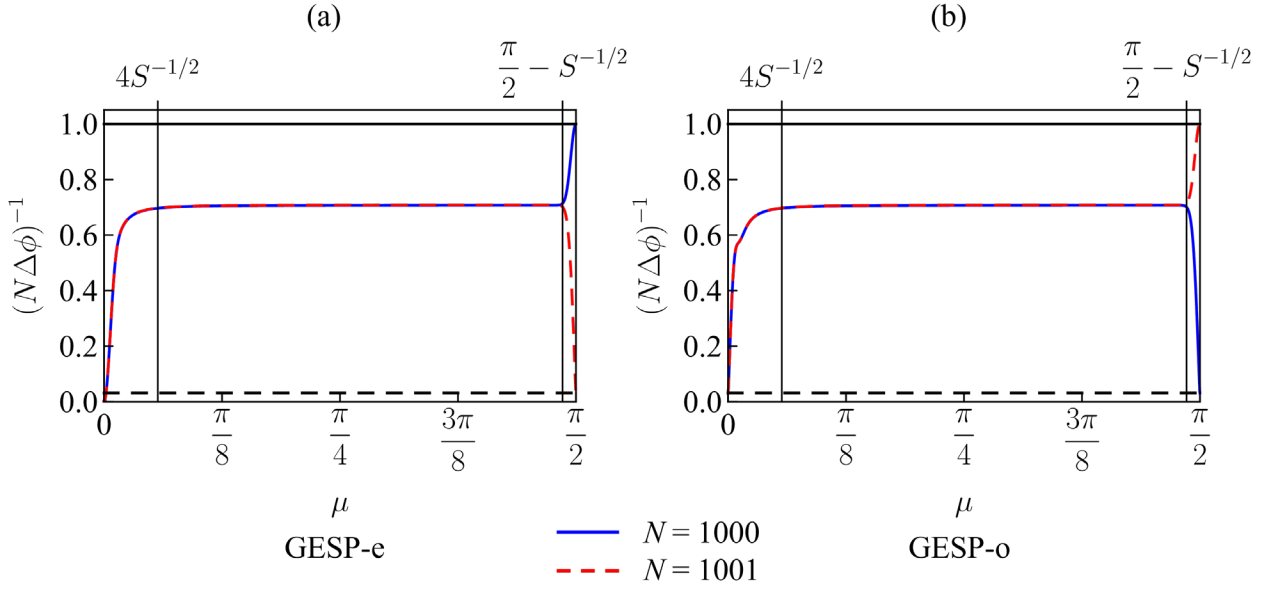


Figure 7. Sensitivity of (a) the GESP-e and (b) the GESP-o for $N=1000$ (blue solid) and 1001 (red dashed) normalized to the Heisenberg limit and the interval $4S^{-1/2} \leq \mu \leq (\pi/2 - S^{-1/2})$ where the sensitivity is approximately the Heisenberg limit divided by $\sqrt{2}$. The horizontal solid black line is the Heisenberg limit and the dashed black line is the standard quantum limit.

5. Phase magnification and noise amplification

While the sensitivity analyzed in Section 3 indicates the limit of what can be achieved, it is also useful to determine the interplay between phase magnification and noise amplification in the determination of the net enhancement in sensitivity. This is because the degree of noise amplification determines the robustness of a given protocol against excess noise [11]. To see why, note that the sensitivity including excess noise can be expressed as:

$$\Delta\phi^{-1}\Big|_{\phi=0} = \frac{\left| \partial_{\phi} \langle S_{x(y)} \rangle \right|}{\sqrt{\Delta S_{\text{QPN}}^2 + \Delta S_{\text{EN}}^2}} \Big|_{\phi=0} \quad (17)$$

In conventional use of the OATS, the quantum projection noise is demagnified, thus making the system extremely sensitive to excess noise. In the case of the CESP, the quantum projection noise remains unchanged, thus increasing the robustness against excess noise, when compared to the case employing conventional OATS. In the case of the SCSP, the quantum projection noise is amplified by a factor of \sqrt{N} , thus making it far more robust against the excess noise than the CESP. As such, it is imperative to understand the degree of quantum projection noise amplification for the GESP.

For a protocol that does not make use of spin squeezing, the signal is $S \cos \phi$, and the noise is $\sqrt{S/2} |\sin \phi|$. For a general case, in the proximity of $\phi = 0$, any signal symmetric about $\phi = 0$ can be approximated by $S \cos(M\phi)$ and the noise by $A\sqrt{S/2} |\sin(M\phi)|$, where the parameter M represents the phase magnification factor (PMF), and the parameter A represents the noise amplification factor (NAF). The net enhancement of the sensitivity is given by (M/A) [11]. In the case of a protocol without spin squeezing, we have $M = A = 1$. For the case where the signal is

anti-symmetric about $\phi = 0$, it is also possible to define equivalent values of the PMF and the NAF, as we will show later. We now use this generalized framework to compare the spin-squeezing protocols described in this paper.

Consider first the PMF and the NAF for the two versions of the SCSP. For clarity of discussion, we introduce here the following terminology. The cases when SCSP-e is applied to the even N case or SCSP-o is applied to the odd N case are denoted as parity-matched SCSPs. On the other hand, the cases when SCSP-e is applied to the odd N case or SCSP-o is applied to the even N case are denoted as parity-crossed SCSPs. For the parity-matched SCSPs, the signal is $S \cos 2S\phi$, and the noise is $S |\sin 2S\phi|$ [28]. Thus, for the parity-matched SCSPs, the PMF is $M = 2S = N$ and the NAF is $A = \sqrt{2S} = \sqrt{N}$. The net enhancement of the sensitivity is then $(M/A) = \sqrt{N}$, reaching the Heisenberg limit. For parity-crossed SCSPs, the signal and noise are a little more complicated. For the SCSP-o applied to even N , the final state is [17]

$$|\psi\rangle = e^{i\mu S_x^2} e^{-i\phi S_y} e^{-i\mu S_z^2} \left| \frac{\pi}{2}, 0 \right\rangle = \frac{1}{2} \left[\left(\left| \frac{\pi}{2} - \phi, 0 \right\rangle + \left| \frac{\pi}{2} + \phi, 0 \right\rangle \right) + (-1)^S i \left(\left| \frac{\pi}{2} + \phi, \pi \right\rangle - \left| \frac{\pi}{2} - \phi, \pi \right\rangle \right) \right] \quad (18)$$

The signal is thus given by:

$$\begin{aligned} \langle \psi | S_x | \psi \rangle &= \langle \psi | R_y \left(\frac{\pi}{2} \right) S_z R_y \left(-\frac{\pi}{2} \right) | \psi \rangle \\ &= \frac{1}{4} \left[\left(\langle -\phi, 0 | + \langle \phi, 0 | \right) \right. \\ &\quad \left. - (-1)^S i \left(\langle \pi + \phi, \pi | - \langle \pi - \phi, \pi | \right) \right] S_z \left[\left(| -\phi, 0 \rangle + | \phi, 0 \rangle \right) \right. \\ &\quad \left. + (-1)^S i \left(| \pi + \phi, \pi \rangle - | \pi - \phi, \pi \rangle \right) \right] \quad (19) \\ &= \frac{1}{2} \left(\text{Re} \left(\langle -\phi, 0 | S_z | \phi, 0 \rangle \right) - \text{Re} \left(\langle \pi + \phi, \pi | S_z | \pi - \phi, \pi \rangle \right) \right) \\ &= S \cos^{2S-1} \phi \end{aligned}$$

Using a similar analysis, it can be shown that the result of Eq. (19) is also valid for the SCSP-e applied to odd N . The interference fringes of the SCSP-e and the SCSP-o for $N = 20$ and 21 are shown in Figure 8. In the proximity of $\phi = 0$, the signal for the parity-crossed SCSPs can be expressed as

$$\langle \psi | S_x | \psi \rangle = S \left[1 + \frac{1}{2} \left(\phi \sqrt{S - \frac{1}{2}} \right)^2 \right] + \mathcal{O}(\phi^4) = S \cos \left(\phi \sqrt{S - \frac{1}{2}} \right) + \mathcal{O}(\phi^4) \quad (20)$$

which agrees with the result shown in Eq. (10). The noise in proximity of $\phi = 0$ calculated with Eq. (11) is

$$\Delta S_x = \sqrt{\frac{S}{2}} \left(S - \frac{1}{2} \right) |\phi| + \mathcal{O}(\phi^3) = \sqrt{\left(S - \frac{1}{2} \right) \frac{S}{2}} \left| \sin \left(\phi \sqrt{S - \frac{1}{2}} \right) \right| + \mathcal{O}(\phi^3) \quad (21)$$

Therefore, both the PMF and the NAF are $\sqrt{S-1/2}$, and it is approximately \sqrt{S} in the limit $S \gg$

1. Consequently, there is no enhancement of the sensitivity for the parity-crossed SCSPs.

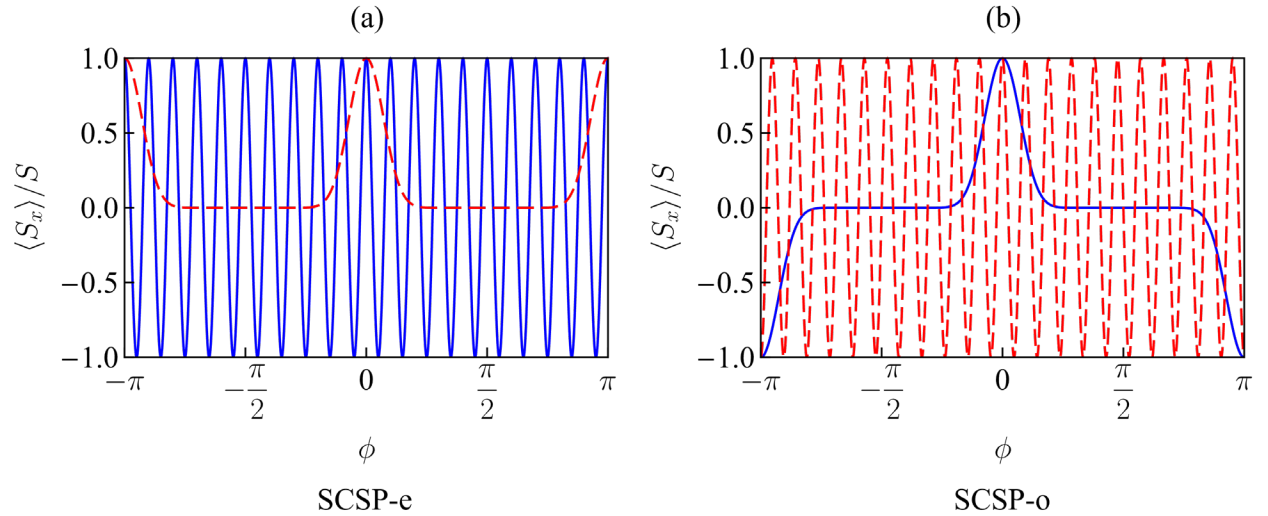


Figure 8. Signal of (a) the SCSP-e and (b) the SCSP-o for $N = 20$ (blue solid) and $N = 21$ (red dashed).

Consider next the case of the CESP, for the optimal value of μ , which is [1] $\text{arccot}\sqrt{2S-2}$. In the proximity of $\phi=0$, the signal of the CESP is $\langle S_y \rangle = [\phi S \sin \mu \cos^{2S-2} \mu + \mathcal{O}(\phi^3)]$. In the limit $S \gg 1$, the optimal value of μ is approximately $1/\sqrt{N}$ and the signal is:

$$\langle S_y \rangle = \phi S \sqrt{\frac{2S}{e}} + \mathcal{O}(\phi^3) = S \sin\left(\phi \sqrt{\frac{2S}{e}}\right) + \mathcal{O}(\phi^3) \quad (22)$$

Although the signal of the CESP is anti-symmetric, it is obvious from Eq. (22) that the effective PMF is $M = \sqrt{N/e}$. The noise in the proximity of $\phi = 0$ is:

$$\Delta S_y = \sqrt{\frac{S}{2}} + \mathcal{O}(\phi^2) = \sqrt{\frac{S}{2}} \cos M\phi + \mathcal{O}(\phi^2) \quad (23)$$

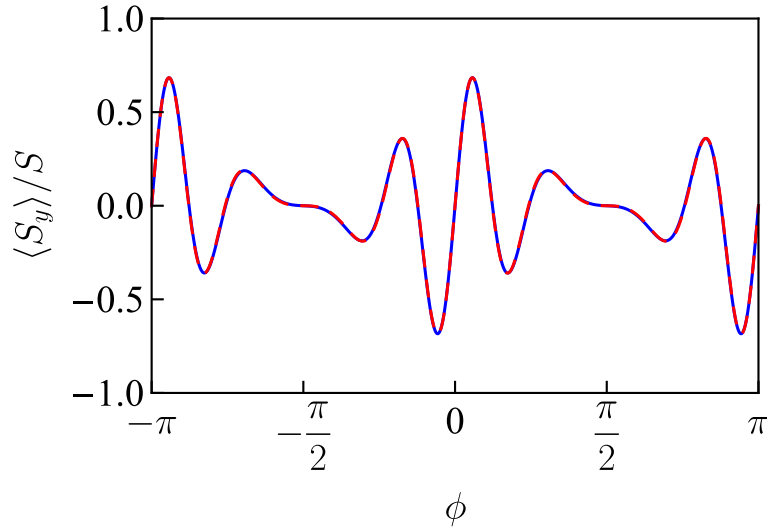


Figure 9. Signal of the CESP for $N=100$ (blue solid) and $N=101$ (red dashed) at the optimal $\mu = \text{arccot}\sqrt{2S-2}$.

Thus, the noise is not amplified at all. Of course, it is evident that these results for the CESP does not depend on the parity of N . For the PMF, this is also evident in Figure 9 where we have shown the actual signals for the CESP for two different parities of N , without any approximations.

Consider next the role of phase magnification and noise amplification in the case of the GESP. According to the discussion in Section 4, in the range of the plateau $4S^{-1/2} \leq \mu \leq (\pi/2 - S^{-1/2})$ and for $S \gg 1$, the signal and the noise for the GESP described by Eq. (10) and Eq. (11) can be expressed as:

$$\langle \psi_{e(o)} | S_x | \psi_{e(o)} \rangle = S \left[1 - \frac{1}{2} (\phi S \sqrt{1 - \cos 2\mu})^2 \right] + \mathcal{O}(\phi^3) = S \cos(\phi S \sqrt{1 - \cos 2\mu}) + \mathcal{O}(\phi^4) \quad (24)$$

$$\Delta S_x = \frac{S^2}{\sqrt{2}} (1 - \cos 2\mu) |\phi| + \mathcal{O}(\phi^3) = \sqrt{S(1 - \cos 2\mu)} \frac{S}{2} \left| \sin(\phi S \sqrt{1 - \cos 2\mu}) \right| + \mathcal{O}(\phi^3) \quad (25)$$

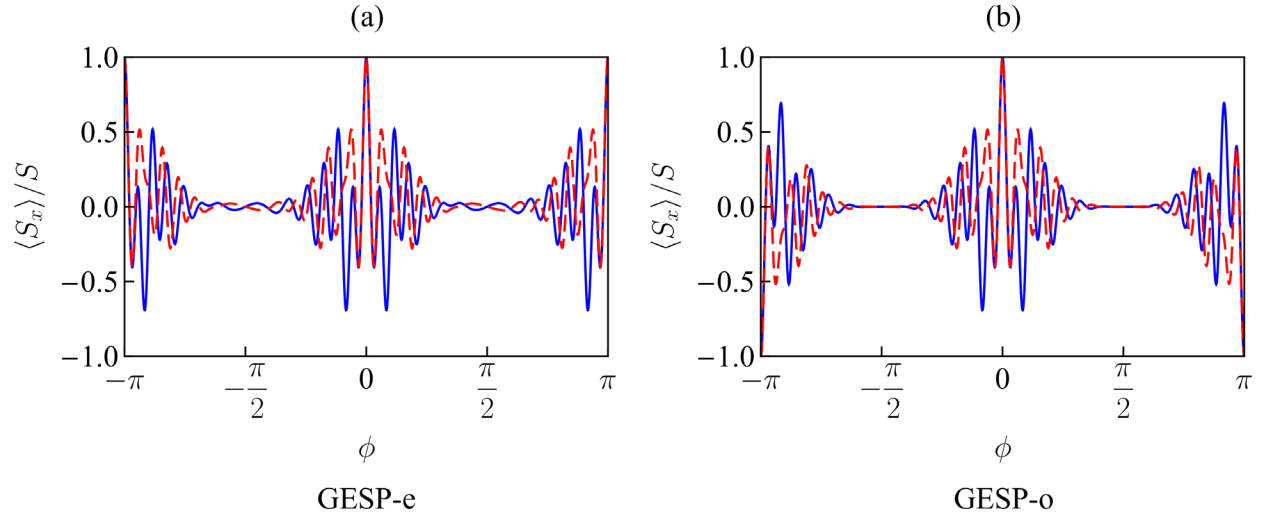


Figure 10. Signal of the (a) GESP-e and (b) GESP-o for $N = 100$ (blue solid) and $N = 101$ (red dashed) at $\mu = \pi/8$.

Compared to the signal and the noise of the protocol without spin squeezing, we can see that for the GESP, the PMF is $M = S\sqrt{1 - \cos 2\mu}$ and the NAF is $A = \sqrt{S(1 - \cos 2\mu)}$. Therefore, the net

enhancement of sensitivity is $(M/A) = \sqrt{S} = \sqrt{N/2}$, yielding the Heisenberg limit within a factor of $\sqrt{2}$. It should be noted that Eqs. (24) and (25) are valid for both even N and odd N cases. The signal of the GESP for $N = 100$ (blue solid) and 101 (red dashed) are shown in Figure 10, without any approximations. As can be seen, the central fringe of the signal does not depend on the parity of N .

Taking into account the effect of excess noise, the sensitivity of the GESP in the range of the plateau can be expressed as

$$\Delta\phi^{-1}\Big|_{\phi=0} = \frac{S^2 \sqrt{1 - \cos 2\mu} \sin M\phi}{\sqrt{(S^2/2)(1 - \cos 2\mu) \sin^2 M\phi + \Delta S_{\text{EN}}^2}} \Big|_{\phi=0} \quad (26)$$

However, this expression has the problem that the numerator is zero at $\phi = 0$, so that the sensitivity vanishes in the presence of any excess noise. In fact, this problem emerges with any sensing mechanism that produces a signal that is symmetric around $\phi = 0$. To circumvent this problem for such a system, it is customary to employ the so-called hopping technique [29]. Under this technique, one uses the difference in the signals measured at two non-zero values of ϕ symmetric about $\phi = 0$. Typically, the measurements are made for values of ϕ where $|\partial_\phi \langle S_x \rangle|$ is maximum. According to Eq. (24), $\partial_\phi \langle S_x \rangle$ becomes the maximum at $\phi = \pm \pi/2M$. Since the analytic results are approximate, it is not a priori obvious whether the assumption used in deriving the results of Eqs. (24) and (25) are valid for the values of ϕ . To check this, we have compared the results of Eqs. (24) and (25) with the exact simulation results. These are shown in shown in Figure 11 for $N = 100$ and $\mu = \pi/4$. As can be seen, the results of Eqs. (24) and (25) represent good approximations of the actual signal and noise for $\phi = \pm \pi/2M$, and only deviates for significantly

larger values of ϕ . Additional simulations we have carried out (not shown) indicates that the agreement between the results of Eqs. (24) and (25) and the numerically calculated signal and noise increases with increasing value of μ .

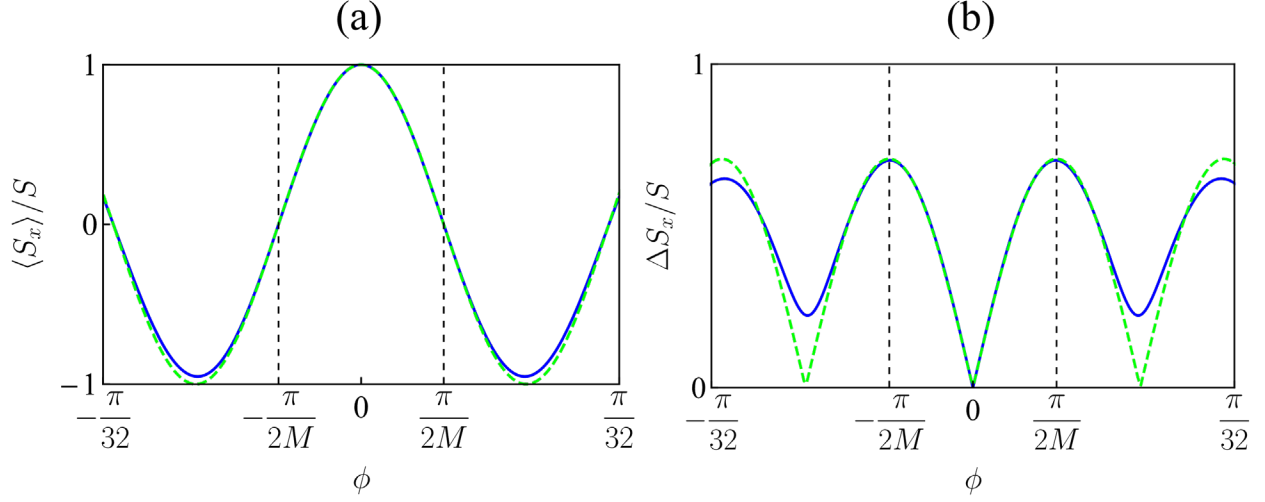


Figure 11. Comparison between the results in Eqs. (24) and (25) (blue solid) with the simulation results (green dashed). (a) Signal (b) Quantum projection noise (robustness)

The signal observed under the hopping technique, with a swing parameter of $\pm \pi/2M$, can be expressed as the expectation value of $S_{\text{hop}}(\varepsilon) = \left[S_x \Big|_{\phi=\varepsilon+\pi/2M} - S_x \Big|_{\phi=\varepsilon-\pi/2M} \right] / 2$, where ε represents the phase shift being measured. Considering that the signal for the GESP is symmetric around $\phi = 0$, and the noises for different values of ϕ are uncorrelated, we can express the phase gradient of the signal as $\partial_\varepsilon \langle S_{\text{hop}} \rangle = \partial_\phi \langle S_x \rangle \Big|_{\phi=\pi/2M}$ and the noise as $\Delta S_{\text{hop}} = \Delta S_x \Big|_{\phi=\pi/2M}$. Therefore, using the hopping technique is equivalent to making measurements at $\phi = \pi/2M$. The sensitivity at $\phi = \pi/2M$ in the presence of the excess noise can then be expressed as:

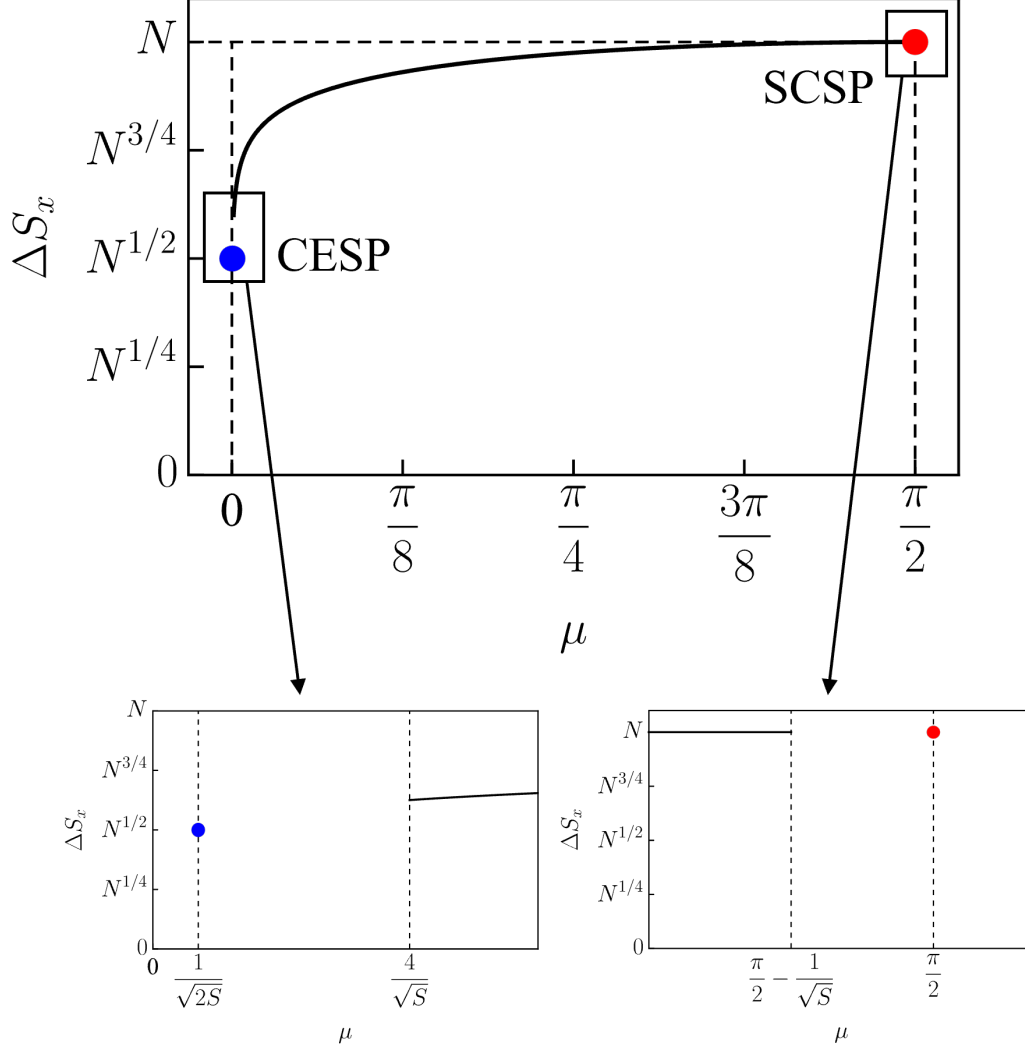


Figure 12. Robustness, which is described by the quantum projection noise, for GESp (black solid curve) in the range of the plateau $4S^{-1/2} \leq \mu \leq (\pi/2 - S^{-1/2})$, CESP for the optimal value of $\mu = (2S)^{-1/2}$ (blue dot), and SCSP (red dot) for $N = 10^6$. The insets show zoomed in views at the two extremes, illustrating the fact that the expressions for the variance in the case of the GESp are plotted only for the plateau over which the enhancement is nearly constant.

$$\Delta\phi^{-1}\Big|_{\phi=\frac{\pi}{2M}} \approx \frac{S^2 \sqrt{1 - \cos 2\mu}}{\sqrt{(S^2/2)(1 - \cos 2\mu) + \Delta S_{\text{EN}}^2}} \quad (27)$$

As can be seen, in the absence of excess noise, the sensitivity employing the hopping technique is the same as what we found earlier when the measurement is made at $\phi = 0$.

The robustness of a protocol against excess noise is defined as the value of ΔS_{ES} for which the sensitivity is reduced by a factor of $\sqrt{2}$. As such, the robustness is given simply by the value of the QPN for any protocol. The QPN of the GESP in the range of the plateau for $N = 10^6$ are plotted (black solid curve) in Figure 12. The red dot shows the QPN for the SCSP and the blue dot for the CESP at the optimal value of $\mu = 1/\sqrt{N}$. Thus, the robustness for the CESP and the protocols without spin squeezing is \sqrt{N} while the robustness for the SCSP is N . For the GESP, in the range of the plateau, the robustness is higher than \sqrt{N} and increases to $\sim N$ as μ increases to $\pi/2$. The insets show zoomed in views at the two extremes, illustrating the fact that the expressions for the variance in the case of the GESP are plotted only for the plateau over which the enhancement is nearly constant.

6. Fragility of a squeezed state

For all the protocols employing one-axis-twist squeezing (OATS) discussed above (namely the SCSP, the GESP, and the CESP), the CSS $\left| \frac{\pi}{2}, 0 \right\rangle$ will go through the squeezing process and the inverse squeezing process. The final state will be restored to $\left| \frac{\pi}{2}, 0 \right\rangle$ in the absence of any phase shift if the atoms are not perturbed in any way between these two steps. However, in practice, there are two obvious possible sources of deleterious perturbations: absorption of stray photons, and collisions with residual background particles. We presume here that with enough care the possibility of absorbing stray photons can be suppressed to a desired degree. Collisions with background particles can also be made negligible by using ultrahigh vacuums produced under

cryogenic conditions [30,31]. For example, in Refs. [32,33,34], which address this issue in the context of attempts to create the macroscopic superposition of nanoparticles, it has been shown that collisions with background particles become negligible for a vacuum of $\approx 10^{-16}$ Torr. Such pressures have been previously realized in cryogenic environments [35]. Here, we estimate the degree of reduction in the fringe contrast expected as a function of the mean number of atoms lost during collisions with background particles. For a given level of vacuum employed in the experiment, such an analysis can serve as a guideline for determining the optimal choice of operating parameters for any of the protocols discussed above.

For the SCSP and the GESP, the quantum operator measured in the end is S_x , with the corresponding signal being $\langle S_x \rangle$. This signal takes its maximum value of $\langle S_x \rangle = S$ in the absence of any collision between the atoms and the background particles. Next, we calculate $\langle S_x \rangle$ in the presence of such collisions. To develop the mathematical model to account for the effect of such collisions, we first define the spin operators for the atoms that have collided with background particles and the atoms that have not. We assume without loss of generality that the first \tilde{N} atoms have collided with background particles. Then the total spin operator for these atoms is denoted as

$$\tilde{\mathcal{S}} \equiv \sum_{j=1}^{\tilde{N}} s_j. \text{ The spin operator for the rest of the atoms is denoted as } \hat{\mathcal{S}} \equiv \sum_{j=\tilde{N}+1}^N s_j. \text{ It is obvious that}$$

collisions that happen before the squeezing process or after the inverse squeezing process simply reduces the effective value of N . As such, these types of collisions are negligible if $\tilde{N} \ll N$. Therefore, we only consider the case where the collisions happen between the squeezing and the inverse squeezing process.

The effect of a collision is modeled as an event under which the atom that has collided with a background particle follows a kinetic trajectory that eludes the inverse squeezing process. Mathematically, the inverse squeezing process is expressed as $\exp(i\mu\widehat{S}_z^2)$ in the presence of the collisions. Therefore, the final state can be expressed as

$$|\psi\rangle = e^{i\mu\widehat{S}_z^2} e^{-i\mu\check{S}_z^2} \left| \frac{\pi}{2}, 0 \right\rangle \quad (28)$$

The quantum operator we measure in the end is \widehat{S}_x because any atoms that has not undergone the inverse squeezing process will not be detected. As shown in detail in Appendix B, the corresponding signal is calculated to be

$$\langle \psi | \widehat{S}_x | \psi \rangle = (S - \check{S}) 2^{-2\check{S}} \sum_{m=-\check{S}}^{\check{S}} C_{m+\check{S}}^{2\check{S}} \cos(2m\mu) \quad (29)$$

where $\check{S} = \check{N}/2$ is the total spin of the atoms that have undergone collisions. For $\mu = 0$, the signal is reduced to $(S - \check{S})$, as expected, corresponding to simple exclusion of the atoms involved in collisions. For $\mu = \pi/2$, which corresponds to the Schrödinger cat state, the signal is zero, for $\check{N} \geq 1$. Accordingly, the Schrödinger cat state is the most fragile to collisions. Thus, if one were to employ the SCSP experimentally, the vacuum level must be such that the probability of even one collision per cycle of the squeezing-unsqueezing sequence is significantly less than unity. We next consider two limiting cases: $\check{N} = 1$ and $\check{N} \gg 1$. For $\check{N} = 1$, the signal is $(\cos \mu)(N - 1)/2$. For $\check{N} \gg 1$, the discrete binomial distribution $2^{-2\check{S}} C_{m+\check{S}}^{2\check{S}}$ is close to the continuous normal distribution $\exp(-m^2/\check{S})/\sqrt{\pi\check{S}}$. If it is additionally satisfied that $\mu \ll 1$, the signal can be approximated as:

$$\langle \psi | \hat{S}_x | \psi \rangle \approx (S - \check{S}) \int_{-\infty}^{\infty} dm \frac{1}{\sqrt{\pi \check{S}}} e^{-\frac{m^2}{\check{S}}} \cos 2m\mu = (S - \check{S}) e^{-\check{S}\mu^2} \quad (30)$$

To avoid significant deterioration of the fringe visibility, the condition necessary is $\check{S}\mu^2 \ll 1$, which corresponds to $\mu \ll 1/\sqrt{\check{S}}$. It can be shown that these results also hold for the CESP.

As noted earlier, an apparatus employing a cryogenic vacuum at the level of $\sim 10^{-16}$ Torr may be suitable for implementing the SCSP, satisfying the condition that the probability of even one collision between the squeezing and unsqueezing processes in each cycle is significantly less than unity. For a vacuum system that may not meet this requirement, one needs ensure that the condition mentioned above (i.e., $\mu \ll 1/\sqrt{\check{S}}$) is satisfied. Thus, the optimal choice of the squeezing parameter for the GESP would be determined by a balance between the fragility against collisions with background particles, and the degree of robustness against excess noise, including those from the OATS process itself.

7. Conclusion

In this paper, we describe the advantages of the Generalized Echo Squeezing Protocol (GESP) over the Conventional Echo Squeezing Protocol (CESP). We point out that there are two different versions of the GESP, denoted as GESP-e and GESP-o, each optimized for one of the two possible parities (even or odd) of the total number of atoms. We present the analytical expression of the sensitivity of both the GESP-e and the GESP-o. The GESP is a generalization of the Schrödinger Cat State Protocol (SCSP) with the value of μ being an arbitrary number rather than $\pi/2$. We find that in the interval $4S^{-1/2} \leq \mu \leq (\pi/2 - S^{-1/2})$, the sensitivity of the GESP is approximately the Heisenberg limit lowered by $\sqrt{2}$. For a large N , this plateau interval is almost the whole range

from 0 to $\pi/2$. Therefore, it is possible to operate a sensor over a wide interval of μ without changing the sensitivity. On the contrary, the CESP only works for a very small interval of μ . The sensitivity of CESP drops to ~ 0 once the value of μ becomes greater than $2S^{-1/2}$, which is a very small number for a large N . We also show that, in contrast to the CESP, the sensitivity of the GESP is close to the quantum Cramér-Rao bound over the whole range of μ , indicating that the information of the phase shift contained in the quantum state is near-optimally extracted for any value of μ . In the interval $4S^{-1/2} \leq \mu \leq (\pi/2 - S^{-1/2})$ and for $S \gg 1$, the central fringe of the signal for the GESP does not depend on the parity of N as well as whether we use the GESP-e or GESP-o. We also show how the enhancement in sensitivity in the case of the GESP is due to a combination of two parameters: the phase magnification factor (PMF) and the noise amplification factor (NAF). As the value of μ increases, both PMF and NAF increase, while keeping the ratio of PMF/NAF essentially constant, yielding a net enhancement of sensitivity that is a factor of $\sqrt{2}$ lower than the Heisenberg limit over the whole plateau interval. An important consequence of this behavior is that the robustness of the GESP against excess noise easily exceeds that of the CESP for a broad range of values of μ . As such, in the context of an experimental study, it should be possible to achieve a net enhancement of sensitivity higher than that for the CESP, under typical conditions where the excess noise exceeds the quantum projection noise for the protocol without spin squeezing. Finally, we have analyzed the fragility of the GESP against collisions with background atoms, and show how a balance between the fragility and the robustness against excess noise would in practice determine the optimal choice of parameters for the GESP.

Appendix A

To find the explicit expression of the signal shown in Eq. (9), we need to calculate $\left\langle \tilde{S}_{x/y}^2 \right\rangle$ and

$\left\langle \tilde{S}_{x/y} S_x \tilde{S}_{x/y} \right\rangle$. With the relations [3] $S_x = S_+ \pm iS_y$, $[S_z, S_{\pm}] = \pm S_{\pm}$, $[S_+, S_-] = 2S_z$, and

$f(S_z)S_{\pm} = S_{\pm}f(S_z \pm 1)$, we can rearrange the terms in the $\left\langle \tilde{S}_{x/y} S_x \tilde{S}_{x/y} \right\rangle$ in the normal order or anti-

normal order, as needed. Then we can do the calculation using the generating functions [26], and

two terms mentioned above are calculated to be

$$\left\langle \tilde{S}_{x/y}^2 \right\rangle = \frac{1}{2} S \left(S + \frac{1}{2} \right) \pm \frac{1}{2} S \left(S - \frac{1}{2} \right) \cos^{2S-2} 2\mu \quad (31)$$

$$\left\langle \tilde{S}_{x/y} S_x \tilde{S}_{x/y} \right\rangle = \frac{1}{2} S \left(S - \frac{1}{2} \right) (S+1) \cos 2\mu \pm \frac{1}{2} S \left(S - \frac{1}{2} \right) (S-1) \cos^{2S-3} 2\mu \pm \frac{1}{2} S^2 \cos^{2S-1} 2\mu \quad (32)$$

Substituting Eqs. (31) and (32) into Eq. (9), we obtain the expression of the signal shown in Eq.

(10), with the vectors in the expression given by

$$\mathbf{a}_{10} = \frac{1}{2} S \begin{bmatrix} -S \left(S + \frac{1}{2} \right) \\ \left(S - \frac{1}{2} \right) (S+1) \\ 0 \end{bmatrix}, \quad \mathbf{a}_{11} = \frac{1}{2} S \begin{bmatrix} 0 \\ \left(S - \frac{1}{2} \right) (S-1) \\ -S \left(S - \frac{1}{2} \right) \\ S \end{bmatrix} \quad (33)$$

and

$$\mathbf{b}_0 = \begin{bmatrix} 1 \\ \cos 2\mu \\ \cos^2 2\mu \end{bmatrix}, \quad \mathbf{b}_1 = \cos^{2S-4} 2\mu \begin{bmatrix} 1 \\ \cos 2\mu \\ \cos^2 2\mu \\ \cos^3 2\mu \end{bmatrix} \quad (34)$$

To calculate the variance of S_x , we also need to calculate $\left\langle \psi_{\circ} \left| S_x^2 \right| \psi_{\circ} \right\rangle$. Similar to Eq. (9), this

expectation value can be expressed as

$$\left\langle \psi_{\circ} \left| S_x^2 \right| \psi_{\circ} \right\rangle = S^2 + \phi^2 \left(\left\langle \tilde{S}_y S_x^2 \tilde{S}_y \right\rangle - S^2 \left\langle \tilde{S}_y^2 \right\rangle \right) + \mathcal{O}(\phi^4) \quad (35)$$

The first term in the parenthesis in Eq. (35) is calculated to be

$$\begin{aligned} \left\langle \tilde{S}_y S_x^2 \tilde{S}_y \right\rangle &= \frac{1}{8} S (2S^2 + 3S - 1) + \frac{1}{2} S \left(S - \frac{1}{2} \right) (S - 1) \left(S + \frac{3}{2} \right) \cos^2 2\mu \\ &\pm \frac{1}{2} S \left(S - \frac{1}{2} \right) (S - 1) \left(S - \frac{3}{2} \right) \cos^{2S-4} 2\mu \pm \frac{1}{4} S \left(S - \frac{1}{2} \right) (5S - 1) \cos^{2S-2} 2\mu \end{aligned} \quad (36)$$

The second term in the parenthesis in Eq. (35) is calculated in Eq. (31). Substituting Eqs. (31) and (36) in to Eq. (35), we have

$$\left\langle \psi_{\circ} \left| S_x^2 \right| \psi_{\circ} \right\rangle = S^2 + \phi^2 (\mathbf{a}_{20} \cdot \mathbf{b}_0 \pm \mathbf{a}_{21} \cdot \mathbf{b}_1) + \mathcal{O}(\phi^4) \quad (37)$$

where

$$\mathbf{a}_{20} = \frac{1}{2} S \left(S - \frac{1}{2} \right) \begin{bmatrix} -\left(S - \frac{1}{2} \right) (S + 1) \\ 0 \\ (S - 1) \left(S + \frac{3}{2} \right) \end{bmatrix}, \quad \mathbf{a}_{21} = \frac{1}{2} S \left(S - \frac{1}{2} \right) \begin{bmatrix} (S - 1) \left(S - \frac{3}{2} \right) \\ 0 \\ -\left(S^2 - \frac{5}{2} S + \frac{1}{2} \right) \\ 0 \end{bmatrix} \quad (38)$$

Then the variance is calculated to be the result shown in Eq. (11), with the vectors in the expression given by

$$\mathbf{a}_{30} = \frac{1}{2}S \begin{bmatrix} S^3 + S^2 + \frac{3}{4}S - \frac{1}{4} \\ -2S(S+1)\left(S - \frac{1}{2}\right) \\ \left(S - \frac{1}{2}\right)(S-1)\left(S + \frac{3}{2}\right) \end{bmatrix}, \quad \mathbf{a}_{31} = \frac{1}{2}S \begin{bmatrix} \left(S - \frac{1}{2}\right)(S-1)\left(S - \frac{3}{2}\right) \\ -2S\left(S - \frac{1}{2}\right)(S-1) \\ \left(S - \frac{1}{2}\right)\left(S^2 + \frac{5}{2}S - \frac{1}{2}\right) \\ -2S^2 \end{bmatrix} \quad (39)$$

Appendix B

Noting that $\mathbf{S} = \widehat{\mathbf{S}} + \check{\mathbf{S}}$ and $[\widehat{\mathbf{S}}, \check{\mathbf{S}}] = 0$, the final state given by Eq. (28) can be further written as

$$|\psi\rangle = e^{i\mu\check{S}_z^2} e^{-i\mu(\check{S}_z + \widehat{S}_z)^2} \left| \frac{\pi}{2}, 0 \right\rangle = e^{-i\mu\check{S}_z^2} e^{-i2\mu\check{S}_z\widehat{S}_z} \left| \frac{\pi}{2}, 0 \right\rangle \quad (40)$$

The signal in the presence of collisions between the atoms and the background particles can then be expressed as

$$\langle \psi | \widehat{S}_x | \psi \rangle = \left\langle \frac{\pi}{2}, 0 \left| e^{i2\mu\check{S}_z\widehat{S}_z} e^{i\mu\check{S}_z^2} \widehat{S}_x e^{-i\mu\check{S}_z^2} e^{-i2\mu\check{S}_z\widehat{S}_z} \right| \frac{\pi}{2}, 0 \right\rangle = \left\langle \frac{\pi}{2}, 0 \left| e^{i2\mu\check{S}_z\widehat{S}_z} \widehat{S}_x e^{-i2\mu\check{S}_z\widehat{S}_z} \right| \frac{\pi}{2}, 0 \right\rangle \quad (41)$$

The last step of Eq. (41) still makes use of the commutation relation $[\widehat{\mathbf{S}}, \check{\mathbf{S}}] = 0$. The next step is

to calculate $e^{-i2\mu\check{S}_z\widehat{S}_z} \left| \frac{\pi}{2}, 0 \right\rangle$. We first note that a CSS can be expressed as

$$|\theta, \varphi\rangle = \left| (\theta, \varphi)' \right\rangle \otimes \left| (\theta, \varphi)'' \right\rangle, \text{ where } \left| (\theta, \varphi)' \right\rangle \equiv \bigotimes_{j=1}^{\check{N}} |\theta, \varphi\rangle \text{ and } \left| (\theta, \varphi)'' \right\rangle \equiv \bigotimes_{j=\check{N}+1}^N |\theta, \varphi\rangle. \text{ Therefore, } \widehat{\mathbf{S}}$$

acts only on $\left|(\theta, \varphi)'\right\rangle$ and \tilde{S} only on $\left|(\theta, \varphi)''\right\rangle$. Next, we expand the two states $\left|(\theta, \varphi)'\right\rangle$ and

$\left|(\theta, \varphi)''\right\rangle$ in the basis of the Dicke collective states [3,25]:

$$\left|(\theta, \varphi)'\right\rangle = \sum_{m_0=-\bar{S}}^{\bar{S}} \left(\cos \frac{\theta}{2}\right)^{\bar{S}+m_0} \left(e^{i\varphi} \sin \frac{\theta}{2}\right)^{\bar{S}-m_0} \sqrt{C_{\bar{S}+m_0}^{2\bar{S}}} \left|(m_0)'\right\rangle \quad (42)$$

$$\left|(\theta, \varphi)''\right\rangle = \sum_{m_1=-\bar{S}}^{\bar{S}} \left(\cos \frac{\theta}{2}\right)^{\bar{S}+m_1} \left(e^{i\varphi} \sin \frac{\theta}{2}\right)^{\bar{S}-m_1} \sqrt{C_{\bar{S}+m_1}^{2\bar{S}}} \left|(m_1)''\right\rangle \quad (43)$$

where $\left|(m_0)'\right\rangle$ is a Dicke collective state for the atoms involved in collisions that satisfies

$\tilde{S}_z \left|(m_0)'\right\rangle = m_0 \left|(m_0)'\right\rangle$, and $\left|(m_1)''\right\rangle$ is a Dicke collective state for the atoms not involved in

collisions that satisfies $\hat{S}_z \left|(m_1)''\right\rangle = m_1 \left|(m_1)''\right\rangle$. Then the expression $e^{-i2\mu\tilde{S}_z} \left|\theta, \varphi\right\rangle$ can be

calculated to be

$$\begin{aligned}
e^{-i2\mu\hat{S}_z\hat{S}_z}|\theta,\varphi\rangle &= \left[e^{-i2\mu\hat{S}_z\hat{S}_z} \sum_{m_0=-\bar{S}}^{\bar{S}} \left(\cos\frac{\theta}{2}\right)^{\bar{S}+m_0} \left(e^{i\varphi}\sin\frac{\theta}{2}\right)^{\bar{S}-m_0} \sqrt{C_{\bar{S}+m_0}^{2\bar{S}}} |(m_0)'\rangle \right] \\
&\otimes \left[\sum_{m_1=-\bar{S}}^{\bar{S}} \left(\cos\frac{\theta}{2}\right)^{\bar{S}+m_1} \left(e^{i\varphi}\sin\frac{\theta}{2}\right)^{\bar{S}-m_1} \sqrt{C_{\bar{S}+m_1}^{2\bar{S}}} |(m_1)''\rangle \right] \\
&= \sum_{m_0=-\bar{S}}^{\bar{S}} \left[\left(\cos\frac{\theta}{2}\right)^{\bar{S}+m_0} \left(e^{i\varphi}\sin\frac{\theta}{2}\right)^{\bar{S}-m_0} \sqrt{C_{\bar{S}+m_0}^{2\bar{S}}} |(m_0)'\rangle \right] \\
&\otimes \left[\sum_{m_1=-\bar{S}}^{\bar{S}} \left(\cos\frac{\theta}{2}\right)^{\bar{S}+m_1} \left(e^{i\varphi}\sin\frac{\theta}{2}\right)^{\bar{S}-m_1} e^{-i2\mu m_0 m_1} \sqrt{C_{\bar{S}+m_1}^{2\bar{S}}} |(m_1)''\rangle \right] \\
&= \sum_{m_0=-\bar{S}}^{\bar{S}} \left[\left(\cos\frac{\theta}{2}\right)^{\bar{S}+m_0} \left(e^{i\varphi}\sin\frac{\theta}{2}\right)^{\bar{S}-m_0} e^{-i2\mu m_0 \bar{S}} \sqrt{C_{\bar{S}+m_0}^{2\bar{S}}} |(m_0)'\rangle \right] \\
&\otimes \left[\sum_{m_1=-\bar{S}}^{\bar{S}} \left(\cos\frac{\theta}{2}\right)^{\bar{S}+m_1} \left(e^{i(\varphi+2m_0\mu)}\sin\frac{\theta}{2}\right)^{\bar{S}-m_1} e^{-i2\mu m_0 m_1} \sqrt{C_{\bar{S}+m_1}^{2\bar{S}}} |(m_1)''\rangle \right] \\
&= \sum_{m_0=-\bar{S}}^{\bar{S}} \left(\cos\frac{\theta}{2}\right)^{\bar{S}+m_0} \left(e^{i\varphi}\sin\frac{\theta}{2}\right)^{\bar{S}-m_0} e^{-i2\mu m_0 \bar{S}} \sqrt{C_{\bar{S}+m_0}^{2\bar{S}}} |(m_0)'\rangle \otimes |(\theta,\varphi+2m_0\mu)''\rangle \quad (44)
\end{aligned}$$

It then follows that

$$\begin{aligned}
&\langle\theta,\varphi|e^{i2\mu\hat{S}_z\hat{S}_z}\hat{S}_x e^{-i2\mu\hat{S}_z\hat{S}_z}|\theta,\varphi\rangle \\
&= \sum_{m_0=-\bar{S}}^{\bar{S}} \left(\cos\frac{\theta}{2}\right)^{2(\bar{S}+m_0)} \left(\sin\frac{\theta}{2}\right)^{2(\bar{S}-m_0)} C_{\bar{S}+m_0}^{2\bar{S}} \left\langle(\theta,\varphi+2m_0\mu)''|\hat{S}_x|(\theta,\varphi+2m_0\mu)''\right\rangle \quad (45)
\end{aligned}$$

Noting that the right side of Eq. (41) is just a special case of the expectation value shown in Eq.

(45), we can easily see that the signal in the presence of collisions given by Eq. (41) is

$$\langle\psi|\hat{S}_x|\psi\rangle = 2^{-2\bar{S}} \sum_{m=-\bar{S}}^{\bar{S}} C_{\bar{S}+m}^{2\bar{S}} \left\langle\frac{\pi}{2}, 2m\mu|\hat{S}_x|\frac{\pi}{2}, 2m\mu\right\rangle = 2^{-2\bar{S}} \sum_{m=-\bar{S}}^{\bar{S}} C_{\bar{S}+m}^{2\bar{S}} \cos 2m\mu \quad (46)$$

References:

¹ Davis, E., Bentsen, G., & Schleier-Smith, M. (2016). Approaching the Heisenberg limit without single-particle detection. *Physical review letters*, 116(5), 053601.

-
- ² Hosten, O., Krishnakumar, R., Engelsens, N. J., & Kasevich, M. A. (2016). Quantum phase magnification. *Science*, 352(6293), 1552-1555.
- ³ Kitagawa, M., & Ueda, M. (1993). Squeezed spin states. *Physical Review A*, 47(6), 5138.
- ⁴ Sørensen, A. S., & Mølmer, K. (2002). Entangling atoms in bad cavities. *Physical Review A*, 66(2), 022314.
- ⁵ Britton, J. W., Sawyer, B. C., Keith, A. C., Wang, C. C. J., Freericks, J. K., Uys, H., ... & Bollinger, J. J. (2012). Engineered two-dimensional Ising interactions in a trapped-ion quantum simulator with hundreds of spins. *Nature*, 484(7395), 489-492.
- ⁶ Sørensen, A., Duan, L. M., Cirac, J. I., & Zoller, P. (2001). Many-particle entanglement with Bose-Einstein condensates. *Nature*, 409(6816), 63-66.
- ⁷ Schleier-Smith, M. H., Leroux, I. D., & Vuletić, V. (2010). Squeezing the collective spin of a dilute atomic ensemble by cavity feedback. *Physical Review A*, 81(2), 021804.
- ⁸ Leroux, I. D., Schleier-Smith, M. H., & Vuletić, V. (2010). Implementation of cavity squeezing of a collective atomic spin. *Physical Review Letters*, 104(7), 073602.
- ⁹ Zhang, Y. L., Zou, C. L., Zou, X. B., Jiang, L., & Guo, G. C. (2015). Detuning-enhanced cavity spin squeezing. *Physical Review A*, 91(3), 033625.
- ¹⁰ It can be shown that the description we present regarding the CESP protocol applied to a Ramsey clock is equivalent to the description of the process presented in reference 1, for example.
- ¹¹ Fang, R., Sarkar, R., & Shahriar, S. M. (2020). Enhancing the sensitivity of an atom interferometer to the Heisenberg limit using increased quantum noise. *JOSA B*, 37(7), 1974-1986. Expanded version of this paper with additional details can be found at <https://arxiv.org/abs/1707.08260>
- ¹² Haine, S. A. (2018). Using interaction-based readouts to approach the ultimate limit of detection-noise robustness for quantum-enhanced metrology in collective spin systems. *Physical Review A*, 98(3), 030303.
- ¹³ Sarkar, R., Kim, M. E., Fang, R., & Shahriar, S. M. (2015). N-atom collective-state atomic interferometer with ultrahigh Compton frequency and ultrashort de Broglie wavelength, with root-N reduction in fringe width. *Physical Review A*, 92(6), 063612
- ¹⁴ Sørensen, A., & Mølmer, K. (2000). Entanglement and quantum computation with ions in thermal motion. *Physical Review A*, 62(2), 022311.
- ¹⁵ Leibfried, D., Barrett, M. D., Schaetz, T., Britton, J., Chiaverini, J., Itano, W. M., ... & Wineland, D. J. (2004). Toward Heisenberg-limited spectroscopy with multiparticle entangled states. *Science*, 304(5676), 1476-1478.
- ¹⁶ Leibfried, D., Knill, E., Seidelin, S., Britton, J., Blakestad, R. B., Chiaverini, J., ... & Wineland, D. J. (2005). Creation of a six-atom ‘Schrödinger cat’ state. *Nature*, 438(7068), 639-642.
- ¹⁷ Leibfried, D., & Wineland, D. J. (2018). Efficient eigenvalue determination for arbitrary Pauli products based on generalized spin-spin interactions. *Journal of Modern Optics*, 65(5-6), 774-779.
- ¹⁸ Monz, T., Schindler, P., Barreiro, J. T., Chwalla, M., Nigg, D., Coish, W. A., ... & Blatt, R. (2011). 14-qubit entanglement: Creation and coherence. *Physical Review Letters*, 106(13), 130506.
- ¹⁹ This magnification factor occurs only for the optimal choice of the squeezing parameter, i.e., $\mu = 1/\sqrt{N}$. When the squeezing parameter is much smaller than this, it can be shown [1,2] that the magnification factor is $\sim N\mu$.
- ²⁰ In principle, the rotation can also be measure by applying a $\pi/2$ rotation around the y-axis, followed by a measurement of S_z , and that is exactly what we do for the GESP-o. To see the distinction between these two approaches, it is instructive to consider the case where all four additional pulses are absent. In that case, use of a $\pi/2$ rotation around the y-axis produces a signal that is of the form $(N/2)\cos\phi$. In contrast, use of a $\pi/2$ rotation around the x-axis produces a signal that is of the form $(N/2)\sin\phi$.
- ²¹ Bordé, C. J. (1989). Atomic interferometry with internal state labelling. *Physics letters A*, 140(1-2), 10-12.
- ²² Kasevich, M., & Chu, S. (1991). Atomic interferometry using stimulated Raman transitions. *Physical review letters*, 67(2), 181.
- ²³ Barrett, B., Geiger, R., Dutta, I., Meunier, M., Canuel, B., Gauguier, A., ... & Landragin, A. (2014). The Sagnac effect: 20 years of development in matter-wave interferometry. *Comptes Rendus Physique*, 15(10), 875-883.
- ²⁴ Sarkar, R., Fang, R., & Shahriar, S. M. (2018). High-Compton-frequency, parity-independent, mesoscopic Schrödinger-cat-state atom interferometer with Heisenberg-limited sensitivity. *Physical Review A*, 98(1), 013636.
- ²⁵ Dicke, R. H. (1954). Coherence in spontaneous radiation processes. *Physical review*, 93(1), 99.

-
- ²⁶ Arecchi, F. T., Courtens, E., Gilmore, R., & Thomas, H. (1972). Atomic coherent states in quantum optics. *Physical Review A*, 6(6), 2211.
- ²⁷ Wikipedia contributors. (2021, May 10). Quantum Fisher information. In Wikipedia, The Free Encyclopedia. Retrieved 19:35, October 10, 2021, from https://en.wikipedia.org/w/index.php?title=Quantum_Fisher_information&oldid=1022484528
- ²⁸ As we have shown in reference 11, the values of the phase magnification factor and the noise amplification factor for the parity-matched SCSPs actually depend critically on what type of detection process is employed. Specifically, if the process of collective state detection is employed, then the results are very different from what we get if the conventional detection method is employed. Here, we are assuming that the detection process is conventional, meaning that the signal is $\langle S_x \rangle$ and the noise is ΔS_x , in order to establish proper comparisons with CESP and GESP.
- ²⁹ Itano, W. M., Bergquist, J. C., Bollinger, J. J., Gilligan, J. M., Heinzen, D. J., Moore, F. L., ... & Wineland, D. J. (1993). Quantum projection noise: Population fluctuations in two-level systems. *Physical Review A*, 47(5), 3554.
- ³⁰ Willems, P. A., & Libbrecht, K. G. (1995). Creating long-lived neutral-atom traps in a cryogenic environment. *Physical Review A*, 51(2), 1403.
- ³¹ Andresen, G. B., Ashkezari, M. D., Baquero-Ruiz, M., Bertsche, W., Butler, E., Cesar, C. L., ... & ALPHA Collaboration. (2011). Confinement of antihydrogen for 1000 seconds. arXiv preprint arXiv:1104.4982.
- ³² Romero-Isart, O. (2011). Quantum superposition of massive objects and collapse models. *Physical Review A*, 84(5), 052121.
- ³³ Romero-Isart, O. (2017). Coherent inflation for large quantum superpositions of levitated microspheres. *New Journal of Physics*, 19(12), 123029.
- ³⁴ Pino, H., Prat-Camps, J., Sinha, K., Venkatesh, B. P., & Romero-Isart, O. (2018). On-chip quantum interference of a superconducting microsphere. *Quantum Science and Technology*, 3(2), 025001.
- ³⁵ Gabrielse, G., Fei, X., Orozco, L. A., Tjoelker, R. L., Haas, J., Kalinowsky, H., ... & Kells, W. (1990). Thousandfold improvement in the measured antiproton mass. *Physical review letters*, 65(11), 1317.